

# Characterisation and manufacturing methods of material extrusion 3D printing composites filaments based on polylactide and nanohydroxyapatite.

Jakub Aniulis<sup>a\*</sup>, Bartłomiej Kryszak<sup>b\*\*</sup>, Michał Grzymajło<sup>b</sup>, Grzegorz Dudzik<sup>a</sup>, Krzysztof M. Abramski<sup>a</sup>, Konrad Szustakiewicz<sup>b</sup>

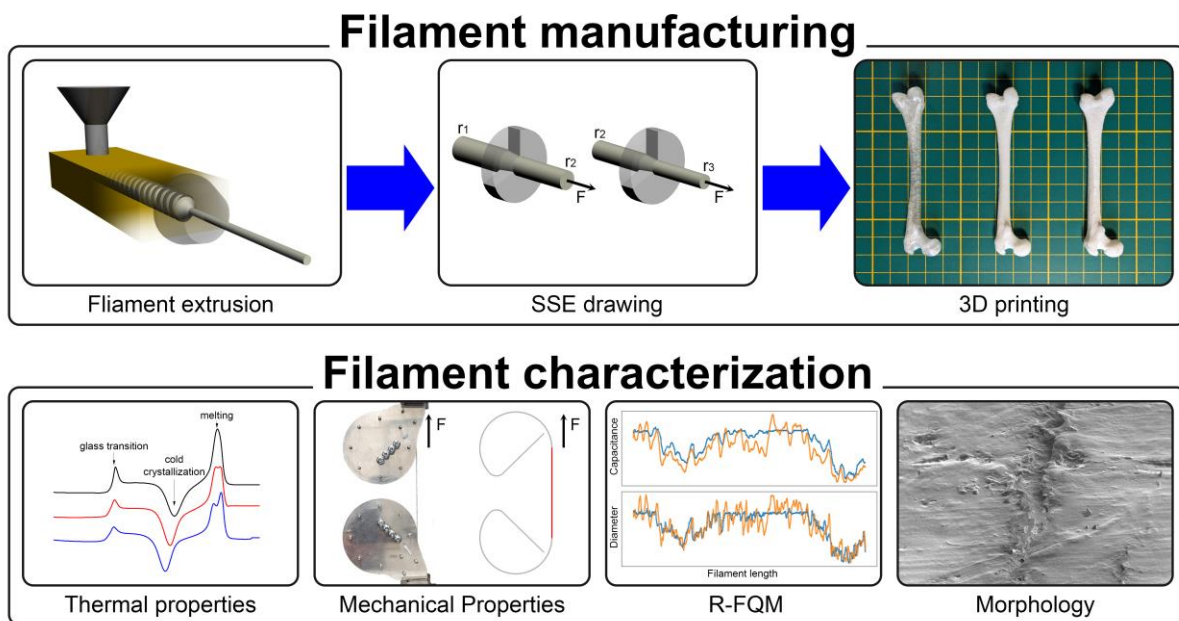
<sup>a</sup>Department of Field Theory, Electronic Circuits and Optoelectronics, Faculty of Electronics, Photonics and Microsystems, Wrocław University of Science and Technology (WUST), Wyb. Wyspiańskiego 27, 50-370, Wrocław, Poland

<sup>b</sup>Department of Polymer Engineering and Technology, Faculty of Chemistry, Wrocław University of Science and Technology (WUST), Wyb. Wyspiańskiego 27, 50-370, Wrocław, Poland

\*Corresponding author: Jakub Aniulis, Department of Field Theory, Electronic Circuits and Optoelectronics, Faculty of Electronics, Photonics and Microsystems, Wrocław University of Science and Technology (WUST), Janiszewskiego 11/17, W12N/K35, Bud. C-2, pok. 210/211, 50-372 Wrocław, Poland, [jakub.aniulis@pwr.edu.pl](mailto:jakub.aniulis@pwr.edu.pl), <https://www.linkedin.com/in/jakub-aniulis/>, <https://www.aniulis.org>

\*\*Corresponding author: Bartłomiej Kryszak, Department of Polymer Engineering and Technology, Faculty of Chemistry, Wrocław University of Science and Technology (WUST), Wyb. Wyspiańskiego 27, 50-370, Wrocław, Poland, [bartlomiej.kryszak@pwr.edu.pl](mailto:bartlomiej.kryszak@pwr.edu.pl)

Graphical abstract:



Highlights:

- Filament diameter reduction by multi-stage solid-state extrusion with a drawing die
- In-process monitoring of filaments characteristics during the manufacturing process
- Properties comparison of PLA composite filament materials (SEM, DSC, TGA, FTIR)
- Low volume PLA-based composite filaments manufacturing with HAP filler
- Tensile test proposal for various materials in the form of filament

Keywords:

Material extrusion filament manufacturing, Diameter characteristic, Filament quality monitor, Structural and thermal properties, Solid-state extrusion with drawing die

## Abstract:

As the pace of scientific research and technological advancement accelerates, there is an increasing demand for rapid on-site prototyping with specific materials. Additive manufacturing through material extrusion 3D printing has emerged as an economically viable solution to this need. The production of custom filaments for this process frequently depends on low-volume filament manufacturing lines. A significant challenge in such production processes is maintaining the quality of the filament throughout its entire length, as this has a considerable impact on the quality of the final printed object. To ensure consistent quality, it is essential to monitor and manage a range of essential properties, including diameter consistency, volume variation, ovality, material homogeneity, compound ratio and the absence of internal and external defects such as air bubbles. This study presents the implementation of a real-time filament quality monitor (R-FQM), which provides detailed insights into the characteristics of the filament during the manufacturing process. In conjunction with a proof-of-concept drawing process for reducing filament diameter by solid-state extrusion, this approach addresses the challenge of maintaining the quality of filaments. The innovative techniques are illustrated in the fabrication of polylactide-based composite filaments with nanohydroxyapatite filler using a multi-stage drawing die solid-state extrusion process. Throughout the manufacturing process, the filaments were characterised using structural and thermal property analyses as well as a proposed tensile test, thereby confirming the effectiveness of the described approach.

## 1. Introduction

As scientific research and the development of new technologies reach unprecedented speeds, the need for rapid onsite prototyping with the desired material is accelerating. The additive manufacturing process of material extrusion 3D printing is gaining popularity as a low-cost solution to meet this need [1]. The low-volume filament manufacturing production line is often used to obtain the desired non-commercial material in the form of filaments [2,3]. One of the challenges in low-volume filament production is maintaining the quality of the filament along its length, which has a major impact on the quality of the output printed object [4]. To address this, it is essential to control and correct key properties of the filament, including diameter and volume variation, ovality, internal and external defects such as air bubbles, and material homogeneity or compound ratio even after extrusion [5]. These properties should be monitored and managed over the length of the filament to ensure consistent quality [6]. In order to address this need, novel methods have been discussed and analysed in this work. These include Real Time Filament Quality Monitoring (R-FQM) [7], filament tensile testing, and filament diameter reduction using Solid State Extrusion (SSE) ([8,9]).

Currently, polylactide (PLA) is one of the most frequently used polymers in additive manufacturing techniques due to its eco-friendliness, good processing properties, and notable mechanical strength [10,11]. Numerous studies are being conducted on the potential use of PLA-based materials in the biomedical field, particularly for the production of biomedical devices such as sutures, screws, pins, or drug release systems [12]. One of the most intensively researched applications of this polymer is in tissue engineering, particularly bone tissue engineering, where, when combined with additives such as hydroxyapatite (HAp), it is intended to support the tissue regeneration process. In PLA-HAp systems, polylactide serves as a bioresorbable matrix, providing the biomaterial with appropriate mechanical strength. Hydroxyapatite whose structure resembles the main mineral component of bone, stimulates the regeneration process due to its osteoconductive properties [13]. Many techniques are used to produce PLA/HAp biomaterials, including thermally induced phase separation [14], electrospinning[15], extrusion [16,17], injection molding [16], and solvent casting [18]. Among them, 3D printing techniques are becoming increasingly popular, especially those based on material extrusion [19,20]. This is due to the possibility of producing materials with good strength, controlled porosity, personalised shape and low equipment costs.

Therefore, there is a need to develop effective methods of producing filaments suitable for 3D printing. The filament manufacturing process begins with the selection of the compound that will form the basis of the material with the desired properties. For material extrusion 3D printing filaments, the main compound is most often polymer [21]. It is common for the polymer to come in the form of pellets, the size of which should be selected according to the filament extruder used for production. It is also important to ensure no moisture in the compounds used for extrusion by drying the materials before the process [22]. Depending on the case, additional pellet grinding or mixing with additional compounds may be carried out before or during material extrusion and in order to ensure good mixing of the ingredients, which will result in greater homogeneity of the output material, additional grinding and extrusion can be carried out afterwards [23]. After the final extrusion process, the filament is produced and can undergo a proposed additional post-processing step. This involves the proposed novel process of drawing the filament through a drawing die [24] for solid-state extrusion to alter its geometry. In order to prepare and monitor the sequence of the post-process treatment, an additional measurement of the filament characteristics can be carried out. When the filament for material extrusion 3D printing is in its final form, its characterisation can give us inside knowledge of its properties, define whether it corresponds to the desired ones and help to estimate the parameters needed for the printing process.

So far, several studies have been published on the production and characterisation of PLA-based filaments with the addition of HAp [13,20,25–27]. In each of the articles cited, the filament production process is based on twin-screw extrusion combined with the winding process. In most cases, the analysis of filament properties is limited only to point measurements of thermal properties, morphology, and possibly chemical structure. To the best of our knowledge, there are no literature reports in which this type of homemade filaments has undergone an in-depth, statistically significant analysis over its entire length. It is also worth noting that the mechanical parameters of the filaments are determined indirectly, i.e. measurements are usually made only for printed samples. Therefore, it would be reasonable to develop a method for measuring the strength of the filaments themselves.

The recently developed method of R-FQM [28] provided insight knowledge of filament characteristics over length during the manufacturing process and, when combined with the proof of concept of material extrusion filament diameter reduction using SSE [29,30], enabled the ability to meet this need. This study demonstrates such an approach with an in-house manufacturing process of PLA-based composite filaments with HAp filler [31]. Furthermore, the utilisation of a multi-stage drawing die [32] solid-state extrusion [33] process is demonstrated, accompanied by the characterisation of the filaments throughout the process with R-FQM. This is supported by reference methods of structural and thermal property analysis, including scanning electron microscopy (SEM), Fourier transform infrared spectroscopy (FTIR), thermogravimetric analysis (TGA), differential scanning calorimetry (DSC) with crystallinity influence, and a novel approach to filament tensile testing (2.9).

## 2. Material and methods

### 2.1. Materials

The base polymer for the production of the filaments was polylactide – PLA Ingeo™ Biopolymer 4043D (pellet form, L-lactide content = 98%,  $M_n = 111$  kDa) supplied by NatureWorks LLC. Hydroxyapatite (HAp) acicular powder ( $\text{Ca}_{10}(\text{PO}_4)_6(\text{OH})_2$ , particle size of  $60 \pm 10$  nm, purity  $\geq 96\%$ ) supplied by Merck was used as the filler. Figure 1 shows an SEM image depicting the morphology of HAp grains, which have a strong tendency to agglomerate.

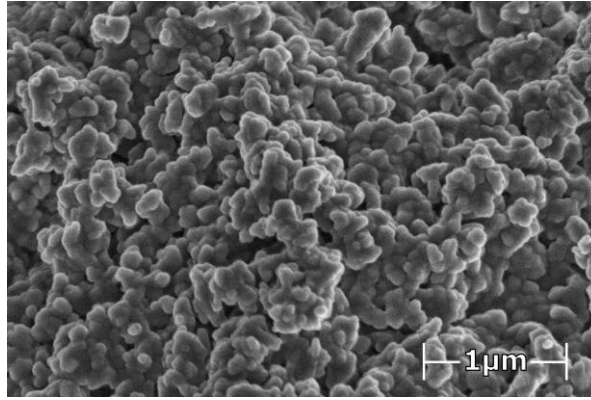


Figure 1 SEM images made with XE-PFIB FEI HELIOS G4 PFIB CXE with TLD detector performed for HAp nano particles.

## 2.2. Filament manufacturing process

The first pre-processing step was to thoroughly dry the components. For this purpose, a Thermo Scientific™ Vacutherm vacuum oven was used. The HAp was dried under vacuum at 100 °C for 24 hours, while the PLA was dried at 70 °C for 24 hours. The next step was to grind the pellet (Cutting Mill SM 300) in order to: (i) obtain smaller polymer granules that are easier to mix with HAp particles, (ii) reduce the size of the granules to facilitate the uptake of material by the screws. Then, in addition to pure PLA, two mixture of PLA with HAp were prepared with 5 and 10 % by weight of hydroxyapatite. After initial mixing, the material was extruded using a Thermo Scientific Process 11 co-rotation Twin-screw Extruder at a temperature of 180 °C in all heating zones and with a screw rotation speed of 200 rpm. The obtained extrudate was cooled on an air track and wound onto a winder. In order to prepare the extruded materials for further processing, they were regranulated using a Brabender Pelletizer. The second extrusion was performed using 3devo Filament Maker Composer with a typical temperature for four heating stages as follows from the inlet to the outlet of the extruder: 180 °C, 185 °C, 190 °C, 175 °C. The Filament Maker's desired outer diameter was set to 1.75 mm, but due to the resulting diameter variation, additional solid state extrusion post-processing ([8,9,34,35]) was required (Chapter 2.3, 3.2). The scheme of the process is shown in Figure 2.

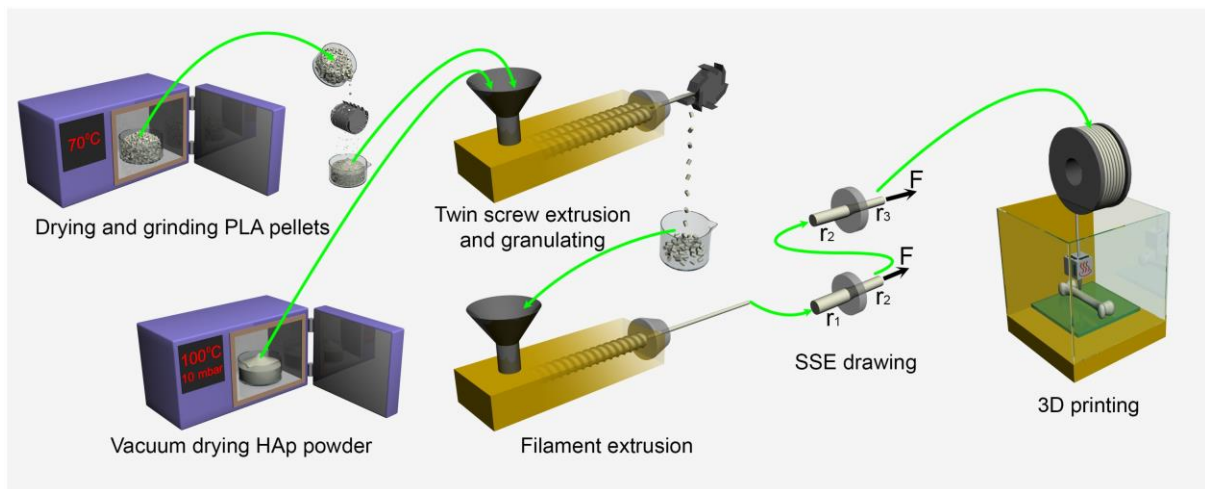


Figure 2 Scheme of material processing carried out for PLA based filaments.

Filaments produced for material extrusion additive manufacturing purposes must have a constant diameter that does not exceed the allowable extruder inlet diameter. In the case of the research objective for material extrusion 3D printers using 1.75 mm filaments, this maximum diameter is most often the diameter of the guiding tube inside the extruder and is equal to 2 mm. However, low-volume material

extrusion of polymer filaments often suffers from imprecise control of the resultant diameter, which can result in significant diameter variation over length. In the case of this research study, due to low volume material extrusion, the produced filament exceeds the maximum diameter ([36], Chapter 3.1) that can be utilised by the 3D printer. In addition, significant variation in diameter over length can result in inferior-quality printed objects [37]. To overcome these challenges, the additional process of solid-state extrusion on the filaments has been proposed.

### 2.3. Filament diameter reduction with solid-state extrusion (SSE)

The solid-state extrusion process is the process of squeezing the base material most often by circular shape to the selected diameter ([8,9,34,35]). To provide such a circular shape which will be rigid enough, dedicated drawing die [24] from a selected material with desired finish is formed for specific diameter [33]. For the material in the form of a filament, the force that moves the filament over the die can be applied before the die inlet (pushing [35]) or after the die outlet (pulling [34]). For filaments, due to the simplicity of the process, only the pulling force has been applied (Figure 2). In the case of such an approach for the polymer filaments, several stages with smaller diameter for each next stage [38] are necessary to avoid breaking the filament during the process [39]. In addition, the diameter differences between each stage must be small enough not to exceed the breaking force and ensure filament continuity [40]. Applying heat to the drawing die [41] or filament was also tested, but the room temperature gave the best effect for the selected material. As the variation in filament diameter was measured (3.1), the final diameter of 1.4 mm was chosen for the filament to ensure a constant filament diameter. For material extrusion 3D printing, such filament with lower but constant diameter can be used for final prints after applying a necessary correction to the extruder from parameters counteracting lower diameter. As a result, each filament was drawn through multiple diameter stages of a tungsten carbide drawing die, starting from a die diameter of 2.5 mm down to 1.4 mm in 0.1 mm decrements.

### 2.4. Nomenclature of samples

Table 1 presents the nomenclature of the samples produced and tested in this work. The first part (PLA) refers to the base polymer, which is the same for all samples. The second part of the name indicates the percentage (w/w) of the HAp filler in the composite. The third part pertains to the SSE process, specifically the diameter of the last drawing die hole used for the filament. Materials marked as 'raw' have not undergone this process and derive their diameter solely from the initial processing. The material described as 'annealed' was additionally subjected to a heating process.

*Table 1 Nomenclature of testes samples*

<b>Sample name</b>	<b>HAp content [w/w%]</b>	<b>Filament diameter [mm]*</b>
PLA_raw	0	as received
PLA_1.4	0	1.4
PLA_1.7	0	1.7
PLA_1.75	0	1.75
PLA_1.75_annealed**	0	1.75
PLA_1.8	0	1.8
PLA_5HAp	5	any
PLA_5HAp_raw	5	as received
PLA_5HAp_1.4	5	1.4
PLA_5HAp_1.7	5	1.7
PLA_5HAp_1.75	5	1.75
PLA_5HAp_1.8	5	1.8
PLA_10HAp	10	any
PLA_10HAp_raw	10	as received
PLA_10HAp_1.4	10	1.4
PLA_10HAp_1.7	10	1.7
PLA_10HAp_1.75	10	1.75
PLA_10HAp_1.8	10	1.8

\* Last used filament treatment of drawing die - Hole diameter

\*\* sample PLA\_1.75\_annealed at 100 °C for 24 hours

## 2.5. Scanning Electron Microscopy (SEM)

SEM imaging was performed using a SEM/XE-PFIB FEI HELIOS G4 PFIB CXE electron microscope. Three types of samples were tested: the initial HAp powder, the cross-section of the filaments, and the surface of the filaments.

The powders were deposited on a carbon flake and then sputtered with a 40 nm layer of carbon. Imaging was performed using a TLD detector at an accelerating voltage of 2 kV and various currents ranging from 50 pA to 0.1 nA.

To visualise the cross-section of the filaments, the samples were cut transversely, and then metallographic microsectioning was performed using a low-temperature resin. In order to analyse the morphology of the filament surfaces, they were mounted in parallel on a microscope table. Then, the surfaces prepared in this manner were sputtered with a 20 nm thick layer of carbon. Imaging was performed using an ETD detector at various accelerating voltages ranging from 2 to 15 kV and currents ranging from 0.1 to 0.4 nA.

## 2.6. Fourier-transform infrared spectroscopy (FTIR)

The FTIR spectra were obtained in ATR mode using a Nicolet iZ10 spectrometer (Thermo Scientific, Waltham, MA, USA), covering the range of 700–4000  $\text{cm}^{-1}$ . Each spectrum consisted of 32 scans and was recorded at a resolution of 4  $\text{cm}^{-1}$ .

## 2.7. Thermogravimetric analysis (TGA)

The thermogravimetric analysis was conducted using the TGA/DSC1 Mettler Toledo analyser. The sample was positioned in a ceramic crucible, and measurements were carried out under a nitrogen atmosphere (flow rate: 60 mL/min) at a heating rate of 10 °C/min, ranging from 25 °C to 600 °C. TGA curves were evaluated using OriginPro ver. 2021 software.

## 2.8. Differential scanning calorimetry (DSC)

The DSC measurements were performed using a Mettler Toledo DSC1 system, coupled with a Huber TC 100 intracooler. Measurements were conducted in three cycles. Initially, the sample was heated within the temperature range of 0–200 °C. Then, after 5 minutes of conditioning in isothermal conditions, the sample was cooled to 0 °C and subsequently heated to 200 °C again. All heating and cooling scans were performed at a rate of 10 °C/min under a nitrogen flow of 60 ml/min.. Experimental data were processed using the generic STARe computer software. For data presentation, the DSC profiles were exported to OriginPro 64 (v. 9.0) as ASCII files and converted into graphs.

## 2.9. Filament tensile testing

The uniaxial static tensile test was conducted using the Instron 5966 universal testing machine. To characterise the strength of the filaments themselves, an aluminum handle was designed and manufactured (refer to Figure 9e), allowing the samples to be fractured in the middle of the measuring section. Measurements were performed at a temperature of 20 °C using a 10 kN load cell with a stretching rate of 10 mm/min. After conducting the tests, the strength parameters for each filament, namely Young's modulus ( $E$ ), tensile strength ( $\sigma_M$ ), yield strength at 0.2% offset ( $\sigma_Y$ ), strain at break ( $\epsilon_B$ ), and toughness ( $U_T$ ), were determined using the Bluehill 3 software and following with calculation from the ISO 527 standard. Each parameter represents an average value obtained from a minimum of 5 measurements.

## 2.10. Real-time filament quality monitor (R-FQM) characteristics

To characterise the filament at different stages of the manufacturing process, an automated non-destructive monitoring of 3D printing filament material properties based on electrical permittivity, longitudinal encoding and diameter multi-axis real-time measurements has been used shown in Figure

3 (detailed R-FQM description in [7]). This measurement methodology allows for obtaining filament characteristics over the length of factors such as capacitive tube capacitance and diameter in selected axis as the filament is passed through various measurement modules synchronised to the motion encoder. This approach allows for calculating filament material properties such as relative electrical permittivity [42], influence of Poisson's ratio, filament roundness, moisture absorption, presence of internal and external defects and component proportions.

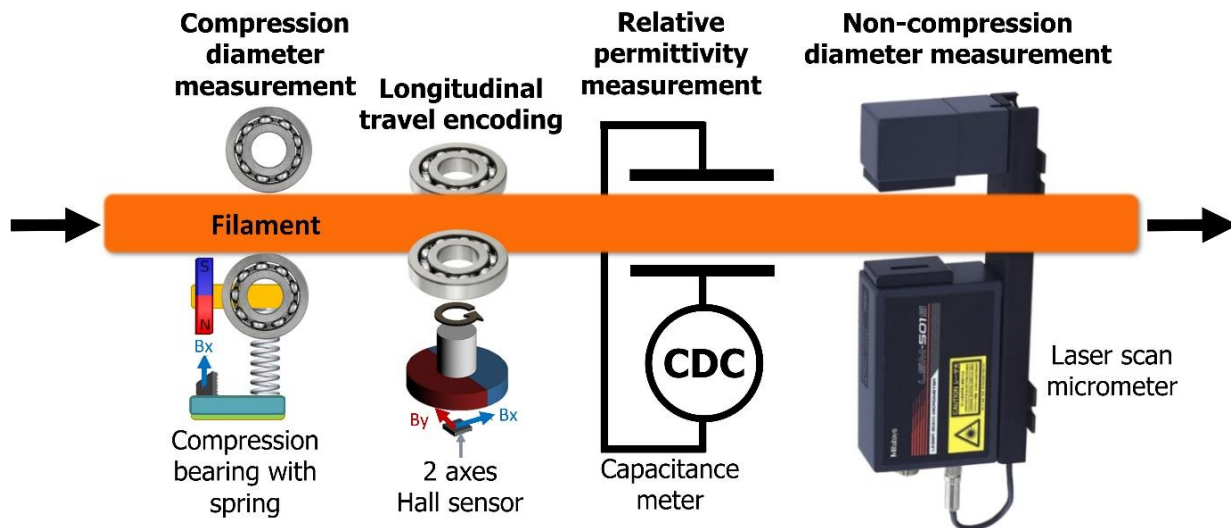


Figure 3 Measurement setup schema [7].

To perform the measurement, the filament is rewound at a constant speed through the setup measurement path while the sensor data is being collected. The sensor readings are mapped to the longitudinal position of the filament fragment using encoder data. The data obtained is then processed to obtain the desired filament characteristics with the necessary correction and material properties. As the diameter is measured by compressing bearings (InFiDEL [43]) with Hall sensors and simultaneously with a non-compressing laser scanning micrometer (LSM, [44]), it is possible to compare the characteristics and estimate the compression influence on the Poisson's ratio 3.7. Based on the corrected diameter and capacitance characteristics after comparison with capacitive tube simulations, it is possible to obtain the relative electrical permittivity of the filament material 3.9.

### 2.11. Determination of the crystallinity using the R-FQM technique

The PLA\_1.75 sample was selected to determine the influence of polymer crystallinity on the measurements obtained using the R-FQM method. Since this material was amorphous, it was heated at 100 °C for 24 hours using a dryer to induce crystallisation. The selected section of the filament was placed in a PTFE tube (inner diameter 1.8 mm, outer diameter 3 mm) to maintain dimensional stability. The obtained effects were measured using FTIR, DSC, R-FQM methods in accordance with the procedures described in subsections 2.62.8, 2.10, respectively.

## 3. Results

### 3.1. Material extrusion filament manufacturing

The material extrusion filament manufacturing process is described and the materials used are described in detail in Chapter 2.2. During the final extrusion of the filament with the 3devo Filament Maker Composer, the extrusion parameters such as the filament winding speed or the filament diameter were monitored and have been used in a feedback loop for better process control. Figure 4 shows the resulting diameter characteristics of the filament over length obtained from the 3devo Filament Maker Composer

optical sensor. The significant diameter variation in small-scale production of filaments is a common problem in filament manufacturing, especially in the case of composite materials [45].

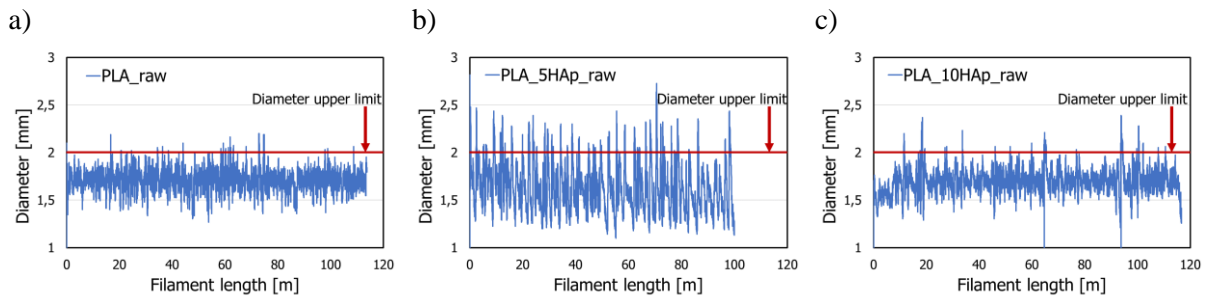


Figure 4 PLA filament characteristics obtained from Filament Maker Precision 3devo filament manufacturing using a built-in optical sensor a) PLA\_raw b) PLA\_5HAp c) PLA\_10HAp

In the case of the material extrusion on 1.75 mm 3D printers, the upper diameter limit is often caused by the leading tube diameter, which exists before the extrusion zone and is often equal to 2 mm [36]. The produced filaments, especially the composites of PLA with HAp, tend to significantly vary in diameter and often exceed this 2 mm limit diameter (Figure 4). It was also observed that the filaments with a higher amount of HAp (PLA\_10HAp, Figure 4 c)) tend to have a lower diameter variation and are more accessible to manufacture than the filament with a lower amount of HAp (PLA\_5HAp, Figure 4 b)). To be able to use the material in material extrusion 3D printers and to reduce the unintended variation of the extruded material volume, it was decided to reduce the filament diameter to 1.4 mm. The choice of this value was dictated by the trade-off between reducing diameter variation and the ability to print the filament with existing extruder designs. The multi-stage solid-state extrusion process with a drawing of the material was selected and developed from several solutions considered (Chapter 2.3, 3.2) and is described in details in Chapter 3.2. In the future application of such an approach, it is recommended that the filament be manufactured with a larger diameter during the manufacturing process extrusion so that the lowest value of the filament diameter characteristics is higher than the desired diameter of 1.75 mm. Then, with the solid state extrusion process, the filament diameter over the entire length can be reduced to a stable value of 1.75 mm with high accuracy even for small-scale filament manufacturing processes.

### 3.2. Filament diameter reduction with SSE using drawing die

Due to the filament diameter variation over length, the maximum allowable diameter for the selected extruder type is exceeded ([36], Chapter 3.1). Also, a large amplitude of diameter variation results in low and unpredictable quality of output prints. To solve these problems, solid-state extrusion in the form of drawing filament through a multi-stage drawing die was applied (described in Chapter 2.3). The filament extruded in the second extrusion stage (2.2) was the basis for the aforementioned solid state extrusion. The setup prepared for the process included several diameters of drawing dies with diameters ranging from 2.5 mm down to 1.4 mm in 0.1 mm decrements, a guide for the filament at the inlet and outlet of the drawing die to ensure that it does not get entangled, a filament pulling unit to ensure that the filament tension is not too high along the length between the drawing die and the pulling device that is the motor for filament drawing, a start filament spool and an end winding filament spool. With this setup, each of the PLA filaments was drawn through a die hole with a decreasing diameter in two different multi-step processes. Most of the filament was prepared for material extrusion 3D printing purposes with the die diameter hole starting from 2.5 mm down 1.4 mm in 0.1 mm decrements. Part of the filament was prepared for the detailed material analysis purposes with the drawing die diameter hole starting from 2.5 mm down 1.8 mm in 0.1 mm step and with the final pass through the 1.75 mm drawing die hole diameter, which is equal to one of the standardised diameters used in material extrusion 3D printing. The die was initially at room temperature, but over time the friction between the PLA and the die would heat it up. Therefore, the filament pulling speed was kept low to ensure that the temperature of the process did not cause the filament to break or deform in an undesirable way.

An example of the R-FQM characteristic of a PLA\_10HAp\_1.75 is shown in Figure 5 a). Corrected sensor readings are assigned to specific filament fragments and presented as a characteristic. Similar characteristics averaged and merged for comparison are shown in other figures such as Figure 5 d) described as multiple merged filament longitudinal characteristics. Based on this the diameter values from different sensors for a specific filament fragment are averaged to give a value which can then be compared as a characteristic of filament over length with other filament characteristics, the same operation is done for capacitance sensors.

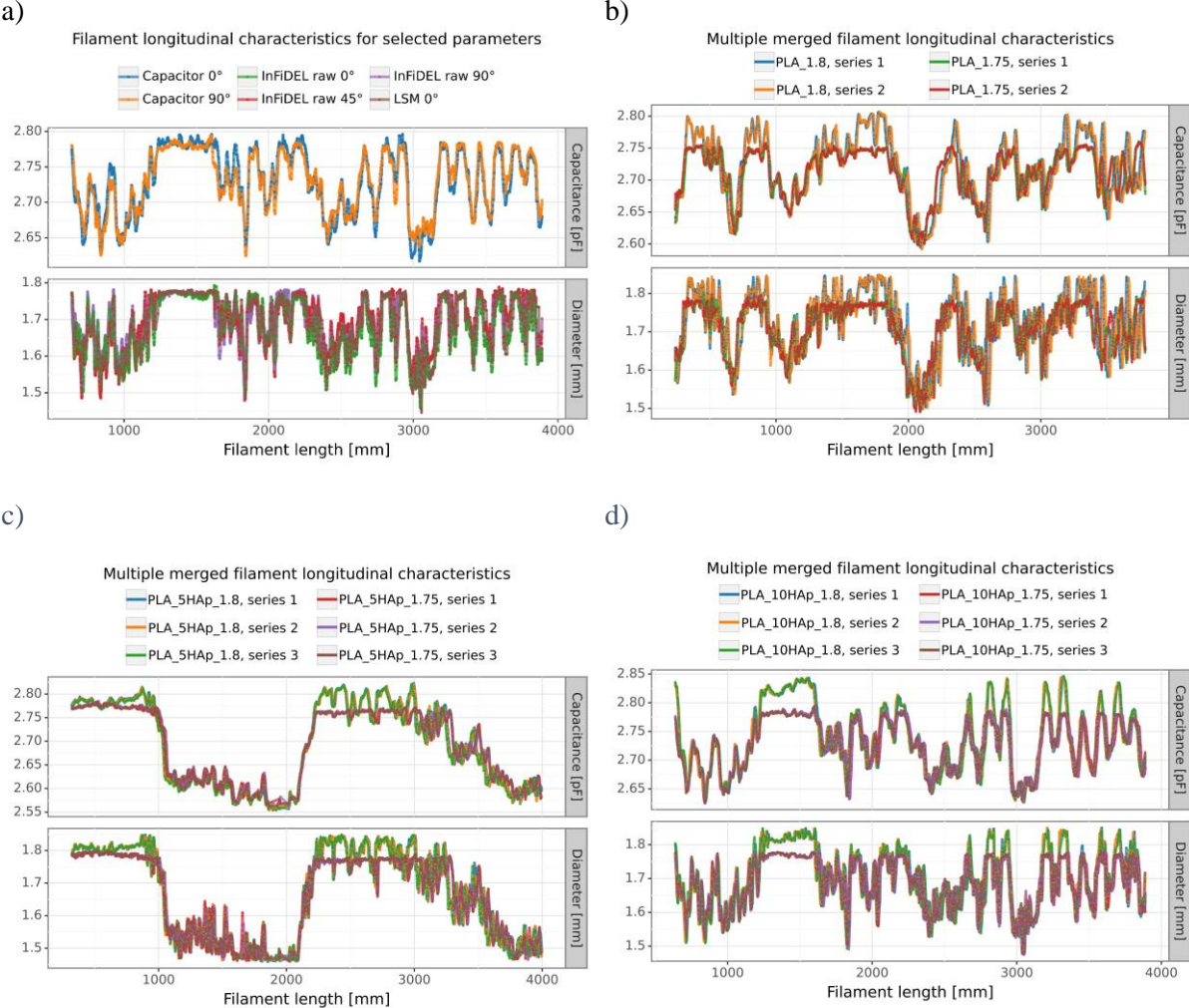


Figure 5 Filament R-FQM characteristics of a) PLA\_10HAp\_1.75 with data from all sensors. Characteristics compared for a single step of solid-state extrusion b) from PLA\_1.8 to PLA 1.75 c) from PLA\_5HAp\_1.8 to PLA\_5HAp\_1.75 d) from PLA\_10HAp\_1.8 to PLA\_10HAp\_1.75.

The process of filament diameter reduction was monitored by characterising the filament for different stages of the process. The maximum diameter accepted by the characterisation device slightly exceeds 1.8 mm, and the monitored stages of filament drawing were selected for optimal measurement parameters. Figure 5 a) is an example of filament with 10% HAp compound final characteristic of diameter and capacitive tube capacitance over length with data from all sensors present measured after drawing the filament through 1.75 mm hole. It shows that the processed sensor data for measuring diameter or capacitance are correlated, where slight differences between each sensor can be further analysed in the case of filament asymmetry (Chapter 3.8). To compare the measured characteristics of the filament, a type of graph called 'Multiple merged filament longitudinal characteristics' has been developed (example Figure 5 d), detailed description in Chapter 2.10). The Figure 5 b) c) d) shows the influence of drawing the filament through the die. In order to obtain the most accurate results, the

characteristics chosen for comparison were those with a diameter of 1.8 mm and a final diameter of 1.75 mm. Three series of characteristic measurements (two in the case of Figure 5 b)) were performed to ensure the repeatability of the measurement setup in the case of the produced filaments.

The flat top fragments of the characteristics show the influence of the drawing dies. The reduction of the filament diameter over the length, where its value exceeds the diameter of the drawing die hole, is clearly visible in these characteristics. In addition, after passing through the die, some of the larger diameter irregularities still leave traces on the characteristic. Also, after passing through the drawing die, the length of the filament fragment increases slightly due to the preservation of solid material volume. These effects are difficult to observe in the PLA\_1.75 after drawing die treatment (Figure 5 b), Figure 12), because passing through holes of different die diameters seems to reduce the friction between the encoder bearing and the filament, resulting in a slight slipping of the filament in the encoder (effect is repeatable). In Figure 5 b) this effect caused the encoded length to decrease by 5% after drawing with a 1.75 mm hole diameter (the x-axis of the characteristics series with drawing through a 1.75 mm hole has been stretched accordingly for comparison) and in Figure 12 after recrystallisation the length increased by a further 12.5% (the x-axis of the recrystallised filament characteristics has been compressed accordingly). This encoder slippage effect was only observed for PLA samples without HAp addition after drawing die treatment and was confirmed by additional sample length measurements without the encoder. Samples with 5% and 10% HAp compounds did not show any slipping effect due to low friction on the surface in relation to the encoder used. The bearing used in the encoder for motion measurement should have additional surface treatment to avoid such effects in future use.

### 3.3. Filament R-FQM characteristics

The filament R-FQM characteristics obtained during diameter reduction for material extrusion 3D printing via solid state extrusion process described in Chapter 2.3, 3.2 with the last pass-over hole diameter equal to 1.7 mm are shown in Figure 6 a). The same filament sample characteristics with reduced diameter for material extrusion 3D printing via solid state extrusion process described in 2.3, 3.2 with last pass over hole diameter equal to 1.4 mm are shown in Figure 6 b). These 1.4 mm diameter filaments were used for printing as they show little variation in diameter over length. In addition, the fragments with significantly smaller diameter were removed for printing purposes (Figure 6 b)). The LSM measurement was used to compare the diameter of the filament samples due to its wide range detection capabilities. Capacitance was averaged between capacitive tubes for ease of comparison.

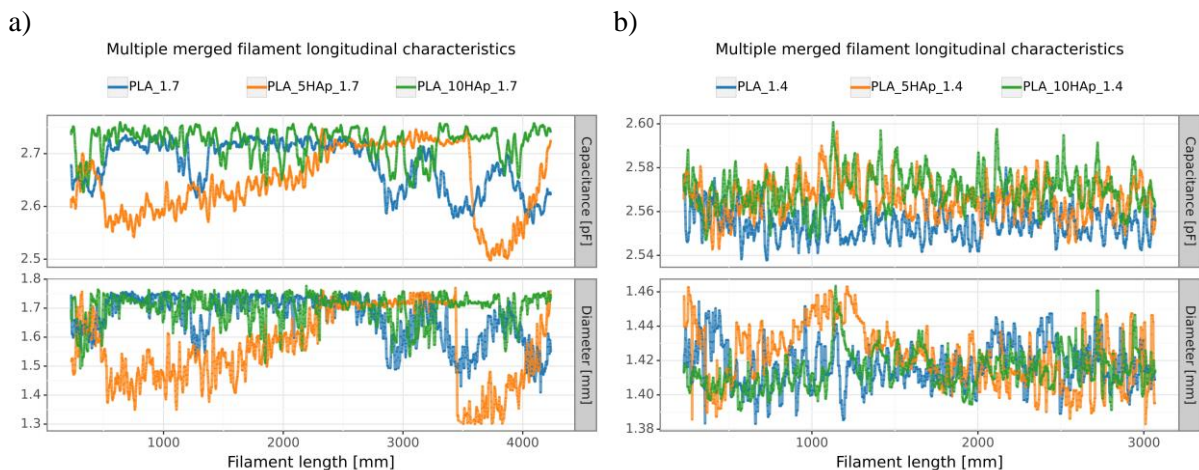


Figure 6 Filament R-FQM characteristics comparison of PLA fragment with various amounts of HAp compound after the samples were drawn with wire drawing dies of various diameters, including a) 1.7 mm drawing die diameter on the last pass and b) 1.4 mm drawing die diameter on the last pass. For the specified amount of HAp compound, filament samples are typical for a) and b) with additional solid-state extrusion treatment for b) described in Chapter 3.3.

The influence of HAp addition on the stability of the extruded filament diameter is shown in Figure 6 a) in a characteristic fragment with higher magnification and resolution compared to Figure 4. It can be observed that the PLA filament with 5% HAp addition has the highest variation of diameter over length. The effects of drawing the filaments in several steps with a drawing die are shown in Figure 6 b). With the post-processing applied, all 1.4 mm filaments have an acceptable low diameter variation with a diameter not exceeding the extruder limit and can be used for material extrusion 3D printing after applying the necessary extrusion multiplier. In addition, it can be observed that the final upper diameter of the filament after passing through the drawing die can exceed the diameter of the drawing die hole (in the case of Figure 5 a), it exceeds 1.7 mm and in the case of Figure 5 b) it exceeds 1.4 mm). This effect is probably caused by non-permanent deformation of the filament, which is stretched while being drawn by the pulling unit and compressed while passing through the drawing die. Once the influence of these phenomena has disappeared, the filament can relax and partially recover from the effects of drawing.

### 3.4. SEM

In order to check the dispersion of HAp particles in PLA filaments after all manufacturing processes the filament cross-section samples were prepared for all 3 types of material in Figure 7 as an image series with an associated letter A. We can see that with a higher amount of HAp addition in PLA material the aggregation of HAp nanoparticles occurs with a visible amount in accordance with declared addition. In 3A, we can see more significant aggregation of HAp in the form of separate islands than in 2A. The 1A image of PLA\_1.4 is referential.

The outer surfaces of the filaments are shown in Figure 7 as a series of images with an associated letter B. Drawing the filament through a multi-stage drawing die resulted in marks on the filament surface. Regardless of the amount of HAp compound longitudinal marks were made along the filament sample visible as a dark lines. These marks may be caused by the etching of the interfibrillar sector formed by amorphous chains [8,46] or the not perfectly smooth outer surface of the drawing dies present in the process and may correspond to die irregularities [8]. Peterlin proposed that as semi-crystalline polymers are drawn, the morphology transitions from a spherulitic structure to a fibrillar structure, with the amorphous chains comprising the inter-fibrillar region, as previously discussed [46,47]. In the case of 3B (10% HAp), the high level of HAp compound addition resulted in additional transverse surface cracks along the filament length. These cracks may be due to the high surface tension between the material and the filament during drawing and the increased brittleness due to the large aggregation of HAp particles in the filament volume [48–50].

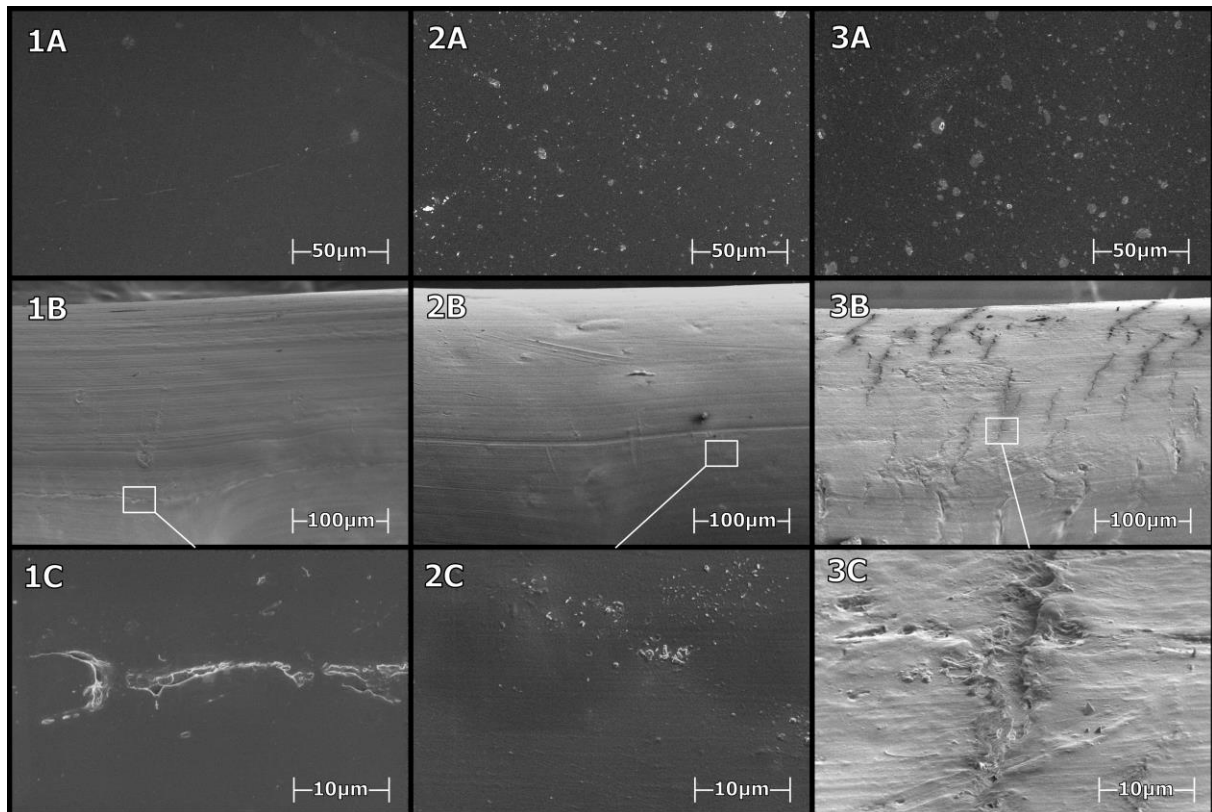


Figure 7 SEM images taken with XE-PFIB FEI HELIOS G4 PFIB CXE with ETD detector of 1.4 mm filaments where numbers are associated to 1) cross-section perspective 2) outer surface 3) selected details, and letters are associated to the HAp addition amount A) PLA\_1.4 B) PLA\_5HAp\_1.4 C) PLA\_10HAp\_1.4

Selected details are shown in Figure 7 as a series of images with an associated letter C. A small crack in the filament without HAp surface is shown in large magnitude 1C. The crack can be caused by the drawing or extrusion processes, but its occurrence on the surface is rare. On 2C HAp, aggregation of the filament cross-section with 5% HAp has been shown. The nanoparticles of the HAp compound are not homogeneously distributed in the filament volume at the micro scale due to their agglomeration [51]. The 3C represents a selected transverse crack in the surface of the filament with 10% HAp. The edge of the crack is raised above the average filament surface and has a sharp structure, as mentioned in [48,52]. Its initiation is edge related to the contact between the drawing die and the filament.

### 3.5. Structural and thermal properties

Thermogravimetric tests were conducted to assess the thermal stability of the filaments produced at 1.4 mm diameter and to estimate the filler content within them. Figure 8 a) illustrates the thermogravimetric curves for the reference PLA material and PLA-based composites containing 5% and 10% filler content by weight. Up to a temperature of approximately 300 °C, all materials demonstrate thermal stability under the given measurement conditions. Hence, the processing temperature range utilised (around 160 °C - 200 °C) appears to be safe regarding polymer degradation. Upon scrutinising the thermal stability parameters outlined in Table 2 ( $T_{-5\%}$ ,  $T_{\text{deriv. peak}}$ ), it becomes evident that the addition of hydroxyapatite results in a marginal enhancement in thermal stability, with the most significant improvement observed in the PLA\_5HAp composite. This observation is further supported by Figure 8 b), wherein the first derivative graph of weight by temperature indicates that the onset peak for pure PLA transpires at lower temperatures, suggesting earlier degradation compared to the composites. A comparable effect of the HAp filler on augmenting the thermal stability of polylactide-based composites has previously been documented in the literature [16]. Upon examining the PLA curve, as expected, at a temperature of 600 °C, the residue amounts to approximately 0.7% - denoting near-complete

decomposition of the organic polymer. For PLA\_5HAp and PLA\_10HAp filaments, this parameter stands at 5.5% and 10.1%, respectively. Presuming the ceramic filler's thermal stability at 600 °C (especially since it underwent drying before processing), the obtained values suggest that the actual filling degrees of the composites closely align with the assumed values.

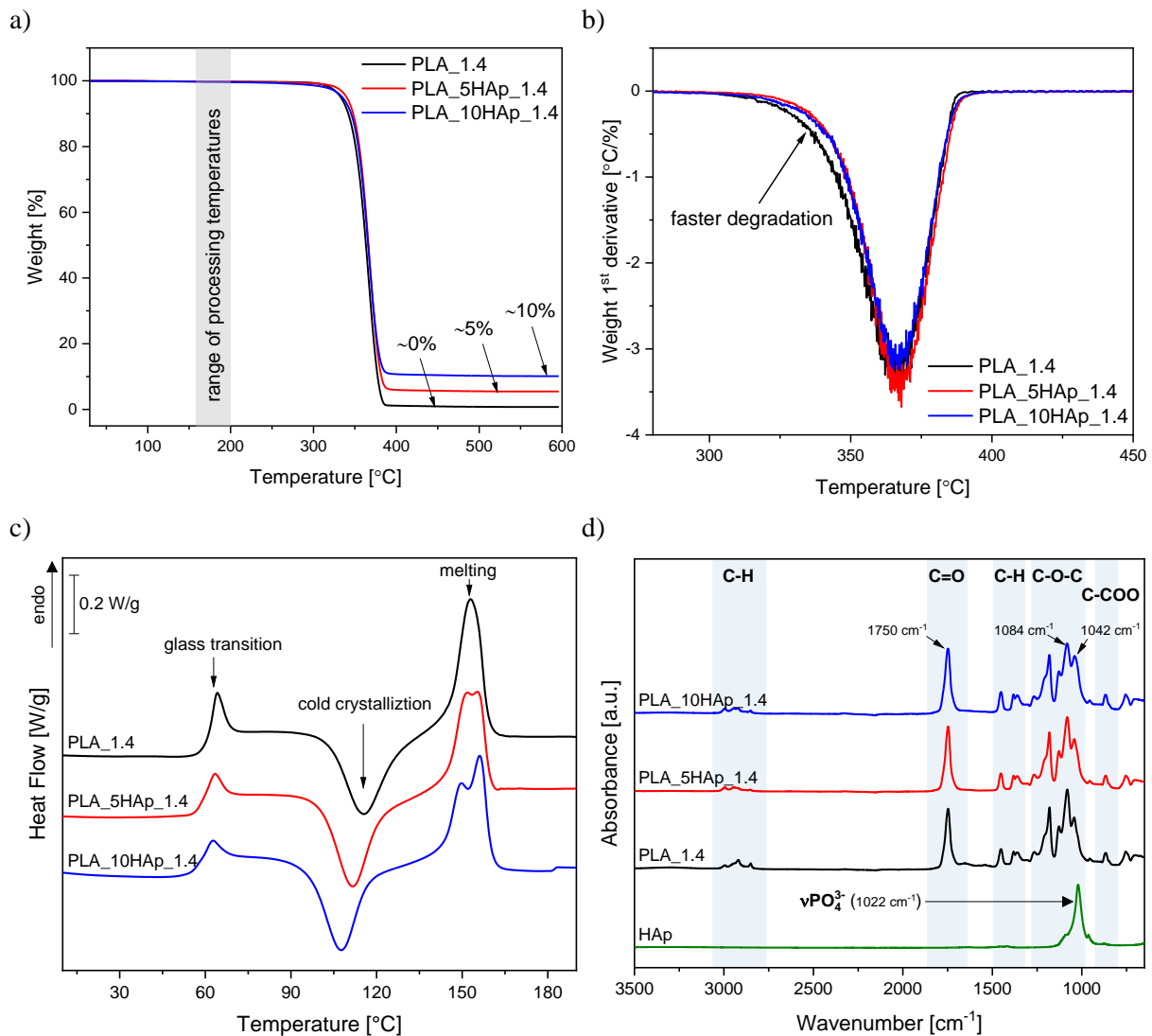


Figure 8 Analysis of the thermal and structural properties of the tested 1.4 mm diameter filaments included: a) TGA thermogravimetric curves, b) DTG curves - the first derivative of mass concerning temperature, c) DSC thermograms from the 1st heating scan, and d) ATR-FTIR spectra of the tested materials.

Figure 8 c) depicts the curves of the first DSC heating scan recorded for the produced 1.4 mm filaments. The trajectory of all curves is similar. When observing from the lowest temperatures, the initial noticeable feature is the inflection of the curve associated with the glass transition of the polymer. As observed, the glass transition is almost invariably accompanied by a distinct relaxation peak linked to macromolecular reorganisation processes. The observed relaxation peak is in agreement with the observation of diameter characteristic comparison where additional diameter variation is gained after heating Figure 12. Subsequently, the next characteristic effect evident in each curve is the exothermic peak attributed to the cold crystallisation of the polymer. Lastly, an endothermic effect is recorded due to polymer melting. Upon analysing the thermal parameters determined using the DSC technique Table 3, one can observe the nucleating effect resulting from the addition of the nanofiller. The incorporation of the filler induces cold crystallisation at lower temperatures. The peak maximum of the  $T_{cc}$  exothermic

peak shifts towards lower temperatures from 115.5 °C (pure PLA) to as low as 107.6 °C (PLA\_10HAp). Alongside the nucleating effect, the addition of HAp influences the formation of crystallites of varying sizes, leading to the splitting of the melting peak. This phenomenon is frequently observed in PLA-based materials [51,53]. For instance, Wang et al. explored PLA composites with the addition of zeolites [51]. By analysing the DSC curves, the values of melting enthalpy  $\Delta H_m$  and cold crystallisation enthalpy  $\Delta H_{cc}$  were also determined. This enabled the calculation (based on the article [14]) of the degree of crystallinity  $X_c$ , which was found to be approximately 0 for each filament, confirming the amorphous nature of the materials. The attainment of filaments with an amorphous structure allowed for the exclusion of the potential impact of crystalline structure on the measurements of electrical permittivity and on the results of mechanical tests.

ATR-FTIR measurements were conducted to verify the chemical structure of the produced 1.4 mm filaments. Figure 8 d) illustrates the infrared spectra obtained for hydroxyapatite powder and the filaments. The spectra of PLA and its composites were normalised to a distinct band corresponding to the stretching vibrations of the carbonyl group  $\nu(\text{C=O})$ , with a maximum at a wavenumber of  $1750 \text{ cm}^{-1}$ . The curve recorded for pure PLA exhibits characteristic features of this polymer [17,54]. In the spectra of composite samples, an increase in filler content leads to a decrease in the intensity ratio between the band with a maximum at  $1084 \text{ cm}^{-1}$  ( $\nu\text{COC}$ ) and the band at  $1042 \text{ cm}^{-1}$  ( $\nu\text{C-CH}_3$ ). This reduction is attributed to the emergence of a new signal from the stretching vibrations of the  $\nu\text{PO}_4^{3-}$  phosphate group originating from HAp molecules ( $1022 \text{ cm}^{-1}$ ) [16].

Table 2 Thermal stability parameters determined from thermogravimetric curves.

Sample	T <sub>-5%</sub> [°C]	T <sub>deriv. peak</sub> [°C]	Residue at 600 °C [%]
PLA_1.4	333.0	365.8	0.7
PLA_5HAp_1.4	340.0	368.2	5.5
PLA_10HAp_1.4	334.9	366.9	10.1

Table 3 Selected thermal parameters of the tested materials derived from 1<sup>st</sup> heating DSC curve.

Sample	T <sub>g</sub> [°C]	T <sub>cc</sub> [°C]	T <sub>m1</sub> [°C]	T <sub>m2</sub> [°C]	$\Delta H_{cc}$ [W/g]	$\Delta H_m$ [W/g]	X <sub>c</sub> [%]
PLA_1.4	59.8	115.5	152.9	-	-27.3	27.7	~ 0
PLA_5HAp_1.4	58.0	111.6	151.8	155.3	-27.5	27.4	~ 0
PLA_10HAp_1.4	57.8	107.6	149.8	156.1	-27.1	27.4	~ 0
PLA_1.75	60.4	115.9	154.2	-	-26.1	25.9	~ 0
PLA_1.75_annealed	62.0	-	156.4	-	-	40.4	~ 43

T<sub>g</sub> – glass transition temperature, T<sub>cc</sub> – temperature of cold crystallisation, T<sub>m1</sub>, T<sub>m2</sub> – melting temperatures,  $\Delta H_{cc}$  – enthalpy of cold crystallisation,  $\Delta H_m$  – enthalpy of melting, X<sub>c</sub> – degree of crystallinity

### 3.6. Mechanical properties

To precisely determine the mechanical properties of the 1.4 mm filaments, a specialised holder dedicated to the uniaxial stretching of the filaments was designed and manufactured (Figure 9 e) ). The conventional approach led to stress accumulation in the material within the testing machine's jaws, resulting in sample fracture outside the measurement section. The proposed method reduces stresses in the sample at the ends of the measurement section, leading to sample cracking in its central part. The efficacy of this approach is evidenced by the strength parameter values closely aligning with literature values for similar materials [16,17]. Figure 9 a) depicts the trends of the curves recorded in the static tensile test. The tested filaments exhibit high brittleness, consistent with the inherent nature of PLA. Generally, hydroxyapatite particles demonstrate good adhesion to the PLA matrix, facilitated by forming hydrogen bonds between C=O and P-OH groups [55,56]. This phenomenon contributes, among other factors, to the increase in Young's modulus upon adding the HAp filler. However, due to the brittle nature of both components, when no other additives are present in the system, the tensile strength or strain at break is reduced [16,57]. The situation differs slightly with the filaments developed in this work. While the PLA\_5HAp\_1.4 material aligns with the trends - exhibiting a higher Young's modulus

than PLA\_1.4 and slightly reduced other parameters, such as  $\sigma_M$ ,  $\sigma_Y$ ,  $\epsilon_B$ ,  $U_T$ , the PLA\_10HAp\_1.4 material shows a clear weakening, also within the meaning of Young's modulus (Table 4). This phenomenon may be attributed to the occurrence of cracks on the surface due to the process of pulling through the eyelet. In the case of pure PLA\_1.4 and PLA\_5HAp\_1.4, no such defects occurred (SEM Figure 7).

*Table 4 Strength parameters of the tested 1.4 mm filaments determined through static tensile testing.*

Sample	E [GPa]	$\sigma_M$ [MPa]	$\sigma_Y$ [MPa]	$\epsilon_B$ [%]	$U_T$ [MPa]
PLA_1.4	$1.07 \pm 0.04$	$64.2 \pm 3.0$	$15.2 \pm 2.1$	$10.5 \pm 1.4$	$4.1 \pm 0.7$
PLA_5HAp_1.4	$1.11 \pm 0.08$	$63.4 \pm 7.0$	$14.3 \pm 1.6$	$10.2 \pm 0.6$	$4.0 \pm 0.4$
PLA_10HAp_1.4	$0.94 \pm 0.08$	$53.3 \pm 5.5$	$13.6 \pm 2.9$	$8.7 \pm 0.4$	$2.7 \pm 0.2$

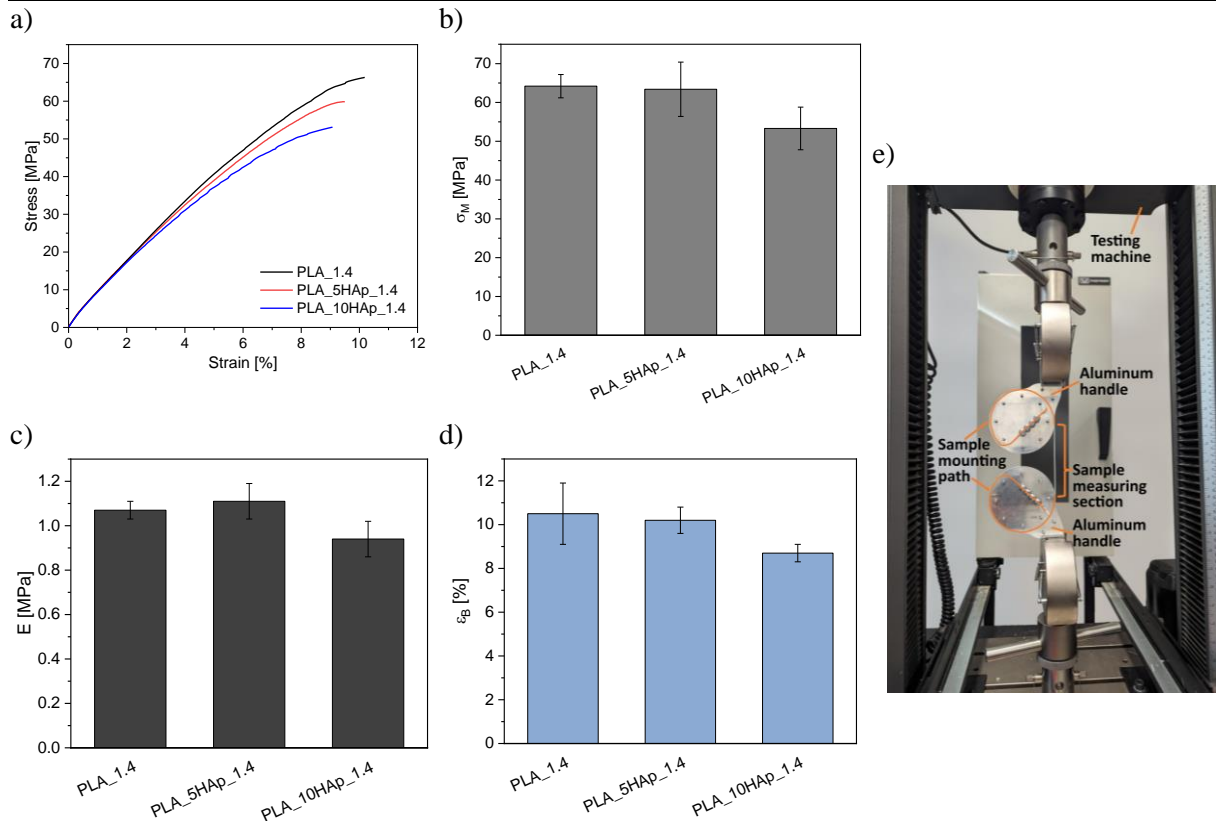


*Figure 9 Analysis of 1.4 mm filament strength in a static tensile test: a) representative stress-strain curves, b) tensile strength ( $\sigma_M$ ) c) Young modulus (E), d) strain at break ( $\epsilon_B$ ), e) a system for uniaxial filament stretching featuring a hand-designed holder specifically tailored for polymer-based filaments.*

### 3.7. Poisson's ratio correction

An analysis was carried out based on the PLA filament R-FQM characteristics from Figure 5 b) c) d) for different levels of HAp compound addition. An illustrative relationship between LSM and InFiDEL measurements for PLA\_5HAp\_1.7 is shown as a density plot in Figure 10 a). This specific PLA sample was later drawn for 3D printing purposes (after all treatment referred to as PLA\_5HAp\_1.4) and the characteristics were measured for the final pass using a 1.7 mm die. The coefficients derived from this relationship, similar to those for PLA\_1.7 and PLA\_10HAp\_1.7, suggest a correlation between LSM and InFiDEL diameter measurements. However, it's worth noting that this relationship may not be applicable to commercially available PLA filaments (probably due to the presence of additional ingredients incorporated for colouring and improved printing properties [7]). Figure 10 b) shows commercial white PLA with various additives used to improve 3D printing properties and experience. To ensure accurate measurements of InFiDEL, an additional correction for the influence of Poisson's ratio must be included in the diameter measurement of commercially available filaments [7,58–62].

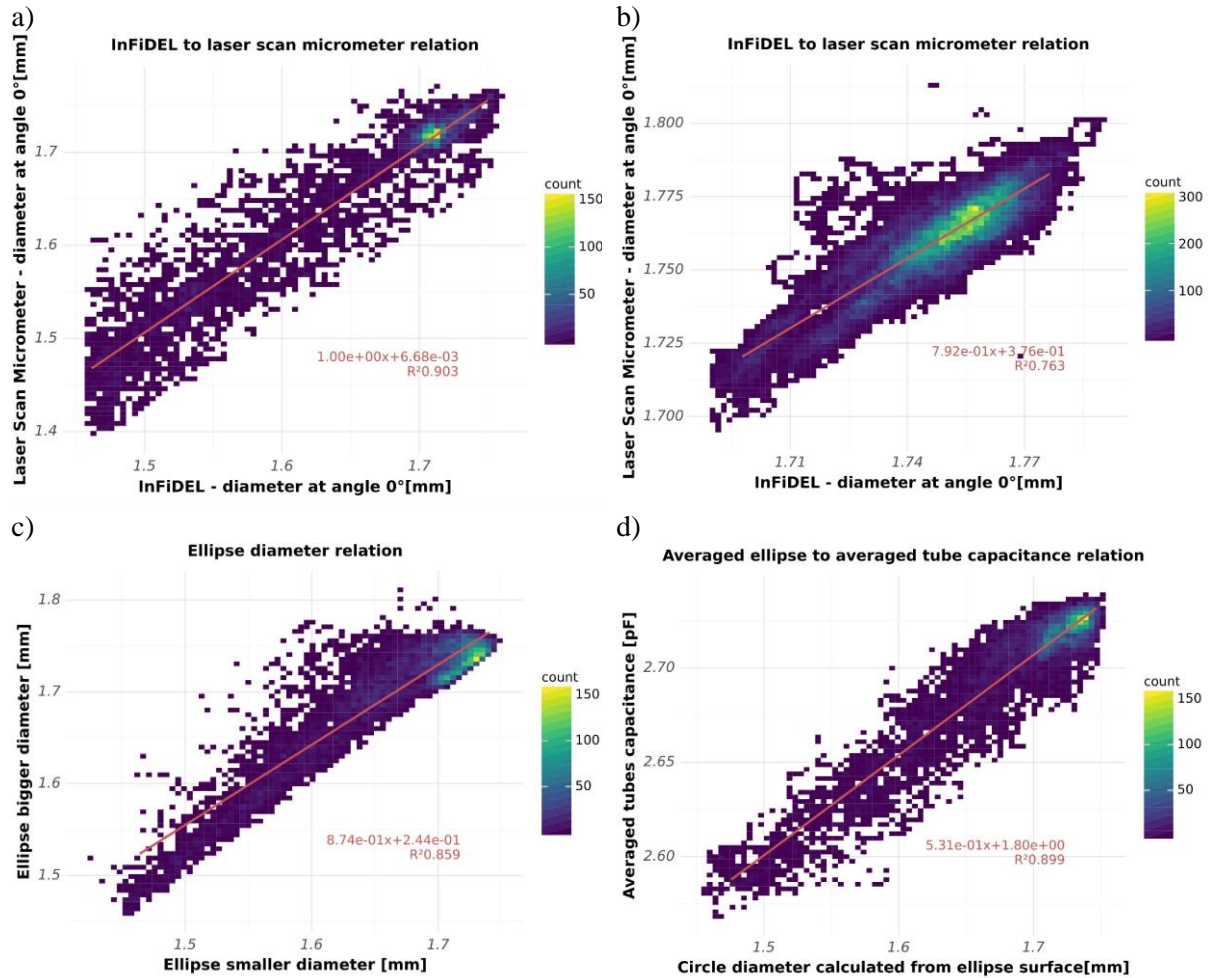


Figure 10 R-FQM density plot of a) Measured diameter relationship of non-compressive laser scan micrometer and compressing bearings measurements for PLA\_5HAp\_1.7 b) Measured diameter relationship of non-compressive laser scan micrometer and compressing bearings measurements for commercial white PLA of declared 1.75 mm diameter c) Estimated relationship of the ellipse diameters based on the characteristics of the PLA\_1.7 d) Relationship between the capacitance tube's substitution capacity and the diameter of the substitute circle for PLA\_1.7

This correction is determined by the coefficient obtained from a linear trend line analysis. In Figure 10 b) this correction can be applied using the equation  $y = 0.792x + 0.376$  (where x is the diameter measured by InFiDEL without Poisson's ratio correction and y is the diameter after correction based on LSM measurements [7]). In the case of PLA\_5HAp\_1.7 produced by the presented process, this equation is  $y = 1x + 0.007$ , which can be approximated to  $y = x$  (which is similar to PLA\_1.7 and PLA\_10HAp\_1.7). This means that in the case of filament made only from used in this paper PLA pellet (Chapter 2.1, 2.2), regardless of the addition of HAp compound from 0 to 10%, the Poisson's ratio correction is not necessary and the material modulus is relatively high. Therefore, Poisson's ratio correction was not applied to all filament diameter characteristics presented in this paper.

### 3.8. Ovality

One of the parameters that can be obtained from a multi-axis diameter measurement is the ovality of the filament. To estimate this relationship, the filament cross-section geometry is approximated by an ellipse [7]. The Figure 10 c) shows the relationship between the smaller and larger ellipse diameter for the PLA\_1.7. The smaller the difference between the smaller and larger ellipse diameter for a specific filament fragment, the better the ovality. In the case of the perfectly oval filament, the graph would be expressed as a single line which symmetrically divides the graph into two parts.

### 3.9. Relative electric permittivity

The parameter that can be estimated based on the combined filament R-FQM characteristics of diameter and capacitive tube capacitance over the length is the relative electric permittivity of the material. The excitation frequency of the capacitance sensor used in the setup is equal to 1.12MHz [8]. To perform this estimation, graph with substitute filament circle diameter calculated from the ellipse surface Chapter 3.8 is placed on the x-axis, and averaged tube capacitance is placed on the y-axis Chapter 2.10. By comparing the generated trend line with the numerical simulation of the capacitive tube Figure 10 d), the relative electric permittivity is estimated (details described in [7]). An example of such a comparison is shown in Figure 10 d) for PLA\_1.7. The data from Figure 10 d) for PLA\_1.7 is presented in Figure 11 together with data from the characteristics of PLA\_5HAp\_1.7 and PLA\_10HAp\_1.7. All filament characteristics shown in Figure 11 were obtained after drawing through a 1.7 mm drawing die Chapter 2.3.

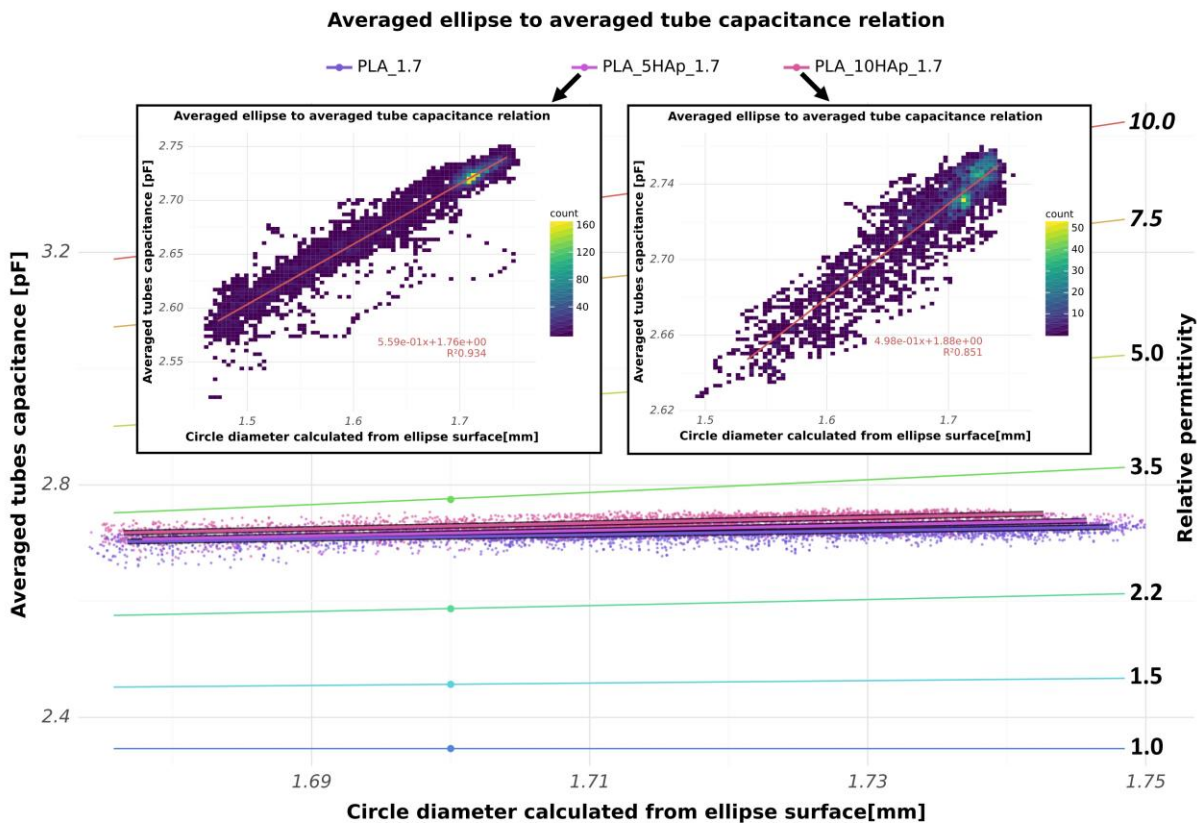


Figure 11 The top two graphs show R-FQM characteristics of PLA\_5HAp\_1.7 (left) and PLA\_10HAp\_1.7 (right). Similar PLA\_1.7 characteristic is shown in Figure 10 d). Below is shown averaged capacitance relationship to substitute diameter normalised to simulation results [8] comparison for the analysed amount of HAp compound in PLA filaments after drawing through a 1.7 mm drawing die.

The addition of different amounts of HAp compound to the PLA filament influences the measured relative electrical permittivity, as shown in Figure 11 and in Table 5. To improve the accuracy of the measurement, the range of diameters used for comparison was optimised to match the high accuracy range of the capacitive tube (the influence of diameter on the accuracy of the capacitive tube is explained in detail in [7]). Table 5 shows the obtained relative permittivity of the materials. Based on the performed comparison of filament characteristics, it can be observed that the relative electric permittivity value is proportional to the amount of HAp compound addition. Based on the measured properties of the PLA\_1.7, its relative electrical permittivity is estimated to be 2.95. This value is highly likely as the

reported relative electric permittivity of PLA varies from 2.7 to 3.1 for frequencies near 1 MHz depending on the material origin [7,63–65]. The effect of recrystallisation is explained in 3.10.

*Table 5 Relative electric permittivity of PLA filaments based on characteristics trend lines compared to simulation (Figure 8, 3.10).*

Material	Relative electric permittivity	Coefficient of determination R <sup>2</sup>
PLA_10HAp_1.7	3.11	0.851
PLA_5HAp_1.7	3.03	0.934
PLA_1.7*	2.95	0.907
PLA_1.75_annealed	2.85	0.789

\* the same relative electric permittivity measured for PLA\_1.75

### 3.10. Crystallinity influence on filament R-FQM characteristics

It was decided to investigate the influence of the degree of crystallinity of PLA\_1.75 on the results of electrical permittivity measurements. A pure PLA\_1.75 sample has been selected for this purpose. Since the initial 1.75 mm filament was amorphous, after the requisite measurements, it was placed in a PTFE tube of suitable diameter (to maintain shape stability - inner diameter 1.8 mm, outer diameter 3 mm) and then heated for 24 hours in a dryer at 100 °C. The effect of heating on the longitudinal characteristics of the filament without HAp addition after drawing through a 1.75 mm drawing die is shown in Figure 12. As the characteristics of the heated sample stretched its length by an additional 12.5% due to insufficient friction between the encoder bearing and the filament after heating (explained in detail in Chapter 2.3, the longitudinal axis was resized accordingly for comparison with the original untreated sample. The average diameter of the sample over its length changed by only 0.3%. As the effect of heating on the longitudinal properties of the filament is not precisely the same along its length, there are some discrepancies between the filament properties.

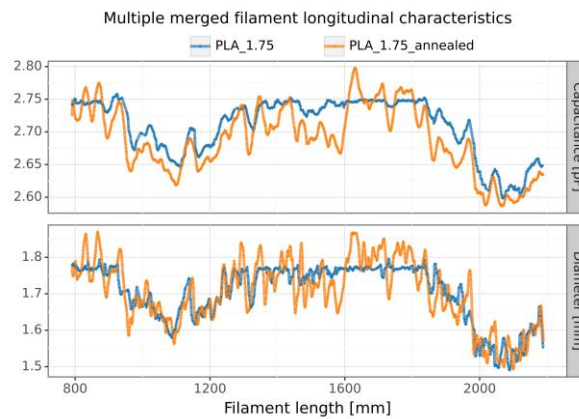


*Figure 12 R-FQM characteristics comparison of PLA sample without HAp compound after drawing through a 1.75 mm drawing die. Characteristics comparison before and after the sample heating for recrystallisation*

Recrystallisation heating also caused an additional change in diameter characteristics. This can be caused by material stress relief or heated material flow. Heating the sample for 24 hours for recrystallisation influences the measured relative electrical permittivity. Figure 13 shows a comparison of the filament characteristics from Figure 12 concerning the simulation. To improve the accuracy of the measurement, the range of diameters used for comparison was optimised to match the high accuracy range of the capacitive tube (the influence of diameter on the accuracy of the capacitive tube is explained in detail in [7]). The estimated relative permittivity value for the filament is given in Table 5. Filament without HAp addition samples used for analysis in Table 5 based on Figure 11 and Figure 13 are



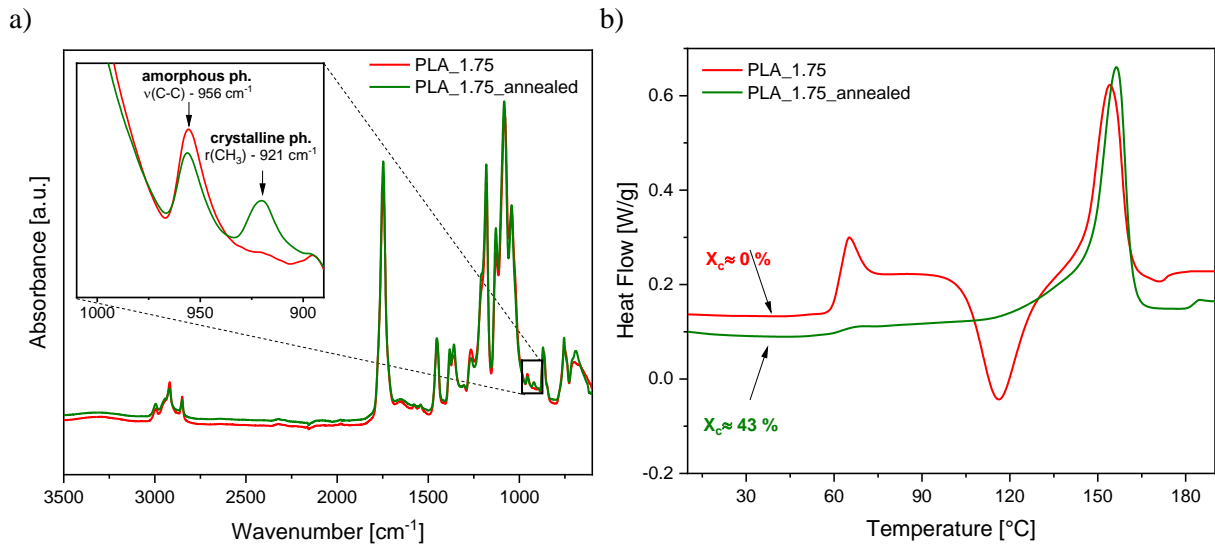


Figure 14 Comparison of the properties of the PLA\_1.75 filament obtained directly from the process and the same filament heated at 100 °C for 24 hours: a) ATR-FTIR spectra, b) DSC curves recorded during the first heating scan.

### 3.11. Material extrusion 3D printing

Hydroxyapatite is highly valued in medical applications due to its utility in bone tissue engineering, which employs additive manufacturing techniques [67]. To examine the printing properties of manufactured filaments of PLA\_1.4, a materials were used to 3D print femur bone scan [68] in 1:5 scale (Figure 15). A Prusa MK3S 3D printer with PrusaSlicer 2.7.4 was employed for this purpose.

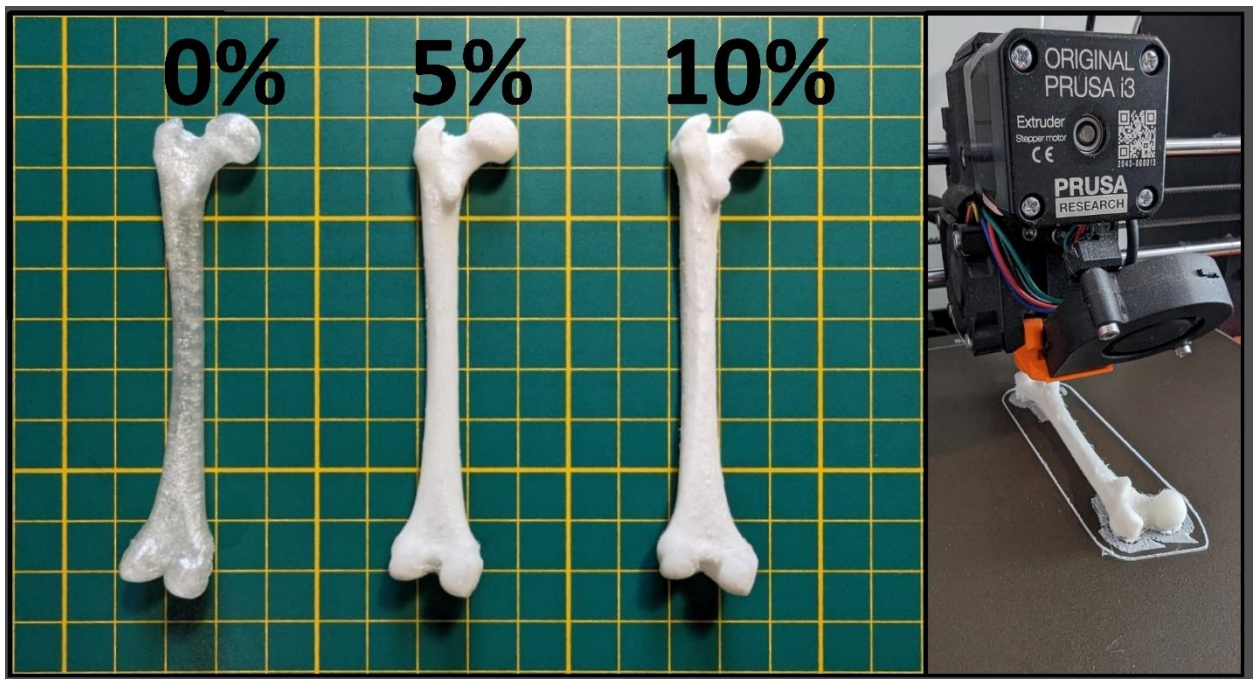


Figure 15 Femur bone scan [68] 3D printed with material extrusion 3D printing. From left, the filament used is: PLA\_1.4, PLA\_5HAp\_1.4, PLA\_10HAp\_1.4. Background scale unit is 1 cm. Prusa MK3S 3D printer was used for printing (on right).

Based on the PLA\_1.4 filament characteristics, as illustrated in Figure 6b, the average diameter of each filament was calculated. The average diameter of the PLA\_1.4 filament was found to be 1.417 mm, while the PLA\_5HAp\_1.4 filament exhibited an average diameter of 1.423 mm, and the

PLA\_10HAp\_1.4 filament had an average diameter of 1.414 mm. The extrusion multiplier for each print was set in accordance with the requisite amount of filament to be extruded during the print. All other slicer settings were identical for all prints, including the extruder nozzle temperature set at 210 °C. The manufacturing of PLA filaments and their subsequent drawing through a multi-stage drawing die enabled the production of high-quality prints despite the smaller 1.4 mm filament diameter (the standard for this type of 3D printer is 1.75 mm) and the use of different material compositions. The femur bone produced using PLA\_1.4 is transparent, whereas the colour of the 3D-printed object is altered to different shades of white when using PLA\_5HAp\_1.4 and PLA\_10HAp\_1.4.

## 4. Conclusion

The physicochemical properties of the produced materials in the form of filaments have been measured by the novel R-FQM technique, which performs characterisation of the filament over its whole length and compared with reference methods based on samples from filament selected points. Obtained results were in agreement for aspects such as HAp compound filler amount or crystallinity influence on material properties and prove the reliability and efficiency of R-FQM technique in the field of filament properties characterisation. The obtained R-FQM properties can also be the basis to evaluate the usability of the material for material extrusion 3D printing in terms of diameter variation and potential problems during the process and can provide necessary correction for printing parameters as extrusion multiplier. The structural and thermal properties of the filament material in its final form were investigated and the results obtained were used to validate the novel properties measurement methods, such as R-FQM or filament tensile testing.

In addition, the life cycle of material extrusion filaments was presented in detail, from the initial stages of raw material ingredients to the final use of the filament in the form of 3D printed objects. For PLA composites, the influence of the HAp compound was analysed with reference to pure PLA filaments, and the properties of the resulting materials were discussed and compared. In addition, the stability of the properties over the filament length was investigated in terms of characteristics. Based on the results, the post-process of filament extrusion could be planned. The presented measuring methods were applied during the process of reducing the filament diameter with the performed multi-stage solid-state extrusion, allowing an insight into the process in the form of compared changes in characteristics.

The process described in the paper allows for producing high-quality 3D prints using filament extrusion 3D printing, regardless of the low-volume filament manufacturing process and the diversity of produced filaments. In the context of future low-volume filament manufacturing, it would be beneficial to first extrude material with a diameter greater than the desired 1.75 mm diameter. This ensures that diameter variation will always be above the desired value, and then diameter can be reduced through solid-state extrusion to achieve the stable desired width. This approach ensures the low variation of diameter with a desired common value, which is used for material extrusion 3D printing. Furthermore, this approach facilitates the production of high-quality prints for low-volume production of designed materials.

## CRedit authorship contribution statement

**Jakub Aniulis:** Conceptualization, Methodology, Software, Formal analysis, Investigation, Resources, Data Curation, Writing - Original Draft, Visualization, Project administration. **Bartłomiej Kryszak:** Conceptualization, Methodology, Validation, Formal analysis, Investigation, Resources, Data Curation, Writing - Original Draft, Visualization. **Michał Grzymajto:** Conceptualization, Methodology, Investigation, Visualization. **Grzegorz Dudzik:** Conceptualization, Validation, Writing - Review & Editing, Supervision. **Krzysztof M. Abramski:** Conceptualization, Validation, Writing - Review & Editing, Supervision, Funding acquisition. **Konrad Szustakiewicz:** Conceptualization, Methodology, Validation, Resources, Writing - Review & Editing, Supervision, Funding acquisition.

## Declaration of competing interest

The authors declare the following financial interests/personal relationships which may be considered as potential competing interests: Jakub Aniulis reports a relationship with Infomat Systemy Komputerowe s.c. that includes: employment. Jakub Aniulis has patent #P.442152 pending to Tortoise Programmer Jakub Aniulis. Jakub Aniulis is realizing an industrial PhD funded by the Ministry of Science and Higher Education in Poland (Grant No. DWD/4/63/2020) in cooperation with Infomat Systemy Komputerowe s.c. and the discussed device is a part of the PhD.

## Acknowledgments

This document is part of the results of Jakub Aniulis industrial PhD research funded by Ministry of Science and Higher Education in Poland (grant No. DWD/4/63/2020). Bartłomiej Kryszak is supported by the Foundation for Polish Science (FNP).

## Bibliography

- [1] B.A. Praveena, N. Lokesh, A. Buradi, N. Santhosh, B.L. Praveena, R. Vignesh, A comprehensive review of emerging additive manufacturing (3D printing technology): Methods, materials, applications, challenges, trends and future potential, in: *Mater Today Proc*, Elsevier Ltd, 2022: pp. 1309–1313. <https://doi.org/10.1016/j.matpr.2021.11.059>.
- [2] N. Vidakis, M. Petousis, N. Michailidis, S. Grammatikos, C.N. David, N. Mountakis, A. Argyros, O. Boura, Development and Optimization of Medical-Grade MultiFunctional Polyamide 12-Cuprous Oxide Nanocomposites with Superior Mechanical and Antibacterial Properties for Cost-Effective 3D Printing, *Nanomaterials* 12 (2022). <https://doi.org/10.3390/nano12030534>.
- [3] A.P. Taylor, C. Velez Cuervo, D.P. Arnold, L.F. Velasquez-Garcia, Fully 3D-printed, monolithic, mini magnetic actuators for low-cost, compact systems, *Journal of Microelectromechanical Systems* 28 (2019) 481–493. <https://doi.org/10.1109/JMEMS.2019.2910215>.
- [4] S. Wickramasinghe, T. Do, P. Tran, FDM-Based 3D printing of polymer and associated composite: A review on mechanical properties, defects and treatments, *Polymers (Basel)* 12 (2020) 1–42. <https://doi.org/10.3390/polym12071529>.
- [5] C. Liu, A.C.C. Law, D. Roberson, Z. (James) Kong, Image analysis-based closed loop quality control for additive manufacturing with fused filament fabrication, *J Manuf Syst* 51 (2019) 75–86. <https://doi.org/10.1016/j.jmsy.2019.04.002>.
- [6] T. Huang, S. Wang, K. He, Quality control for fused deposition modeling based additive manufacturing: Current research and future trends, in: *First International Conference on Reliability Systems Engineering (ICRSE)*, Beijing, China, Doi: 10.1109/ICRSE.2015.7366500, 2015: pp. 1–6.
- [7] J. Aniulis, G. Dudzik, K.M. Abramski, Automated non-destructive 3D printing filament material properties monitoring based on electric permittivity, longitudinal encoding and diameter multi-axes real-time measurements, *Addit Manuf* 84 (2024). <https://doi.org/10.1016/j.addma.2024.104103>.
- [8] J. Walker, M. Melaj, R. Giménez, E. Pérez, C. Bernal, Solid-State Drawing of Commercial Poly(Lactic Acid) (PLA) Based Filaments, *Front Mater* 6 (2019). <https://doi.org/10.3389/fmats.2019.00280>.

- [9] R.S. Porter, New Developments in Solid-State Extrusion, *Journal of Macromolecular Science, Part B* 19 (1981) 377–386. <https://doi.org/10.1080/00222348108015309>.
- [10] J.M. Chacón, M.A. Caminero, E. García-Plaza, P.J. Núñez, Additive manufacturing of PLA structures using fused deposition modelling: Effect of process parameters on mechanical properties and their optimal selection, *Mater Des* 124 (2017) 143–157. <https://doi.org/10.1016/j.matdes.2017.03.065>.
- [11] B. Kryszak, M. Gazińska, P. Gruber, M. Wieczorek, A. Krokos, Mechanical properties and degradation of laser sintered structures of PLA microspheres obtained by dual beam laser sintering method, *The International Journal of Advanced Manufacturing Technology* (2022). <https://doi.org/10.1007/s00170-022-09253-6>.
- [12] V. DeStefano, S. Khan, A. Tabada, Applications of PLA in modern medicine, *Engineered Regeneration* 1 (2020) 76–87. <https://doi.org/10.1016/j.engreg.2020.08.002>.
- [13] M.P. Bernardo, B.C.R. da Silva, A.E.I. Hamouda, M.A.S. de Toledo, C. Schalla, S. Rütten, R. Goetzke, L.H.C. Mattoso, M. Zenke, A. Sechi, PLA/Hydroxyapatite scaffolds exhibit in vitro immunological inertness and promote robust osteogenic differentiation of human mesenchymal stem cells without osteogenic stimuli, *Sci Rep* 12 (2022) 1–15. <https://doi.org/10.1038/s41598-022-05207-w>.
- [14] K. Szustakiewicz, M. Gazińska, B. Kryszak, M. Grzymajło, J. Pięłowski, R.J. Wiglus, M. Okamoto, The influence of hydroxyapatite content on properties of poly(L-lactide)/hydroxyapatite porous scaffolds obtained using thermal induced phase separation technique, *Eur Polym J* 113 (2019) 313–320. <https://doi.org/10.1016/j.eurpolymj.2019.01.073>.
- [15] S.M. Stella, T.M. Sridhar, R. Ramprasath, J. Gim bun, Physio-Chemical and Biological Characterization of Novel HPC ( Hydroxypropylcellulose ): HAP ( Hydroxyapatite ): PLA ( Poly Lactic Acid ) Electrospun Nanofibers as Implantable Material for Bone Regenerative Application, *Polymers (Basel)* 15 (2023) 1–20. <https://doi.org/https://doi.org/10.3390/polym15010155>.
- [16] B. Kryszak, M. Biernat, P. Tymowicz-Grzyb, A. Junka, M. Brożyna, M. Worek, P. Dzienny, A. Antończak, K. Szustakiewicz, The effect of extrusion and injection molding on physical, chemical, and biological properties of PLLA/HAP whiskers composites, *Polymer (Guildf)* 287 (2023) 1–14. <https://doi.org/10.1016/j.polymer.2023.126428>.
- [17] A. Smieszek, K. Marycz, K. Szustakiewicz, B. Kryszak, S. Targonska, K. Zawisza, A. Watras, R.J. Wiglus, New approach to modification of poly (L-lactic acid) with nano-hydroxyapatite improving functionality of human adipose-derived stromal cells (hASCs) through increased viability and enhanced mitochondrial activity, *Materials Science and Engineering C* 98 (2019) 213–226. <https://doi.org/10.1016/j.msec.2018.12.099>.
- [18] A. Prasad, S. Mohan Bhasney, M.R. Sankar, V. Katiyar, Fish Scale Derived Hydroxyapatite reinforced Poly (Lactic acid) Polymeric Bio-films: Possibilities for Sealing/locking the Internal Fixation Devices, *Mater Today Proc* 4 (2017) 1340–1349. <https://doi.org/10.1016/j.matpr.2017.01.155>.
- [19] F. da Luz Belo, E.V. Vasconcelos, M.A. Pinheiro, D. da Cruz Barbosa Nascimento, M.F. Passos, A.C.R. da Silva, M.A.L. dos Reis, S.N. Monteiro, R.T.S.S. Brígida, A.P.D. Rodrigues, V.S. Candido, Additive manufacturing of poly (lactic acid)/hydroxyapatite/carbon nanotubes biocomposites

- for fibroblast cell proliferation, *Sci Rep* 13 (2023) 1–20. <https://doi.org/10.1038/s41598-023-47413-0>.
- [20] V. Namasivayam Sukumaar, S. Arjunan, L.N. Pandiaraj, A. Narayanan, Experimental investigation of 3D printed polylactic acid and polylactic acid – hydroxyapatite composite through material extrusion technique for biomedical application, *Journal of Thermoplastic Composite Materials* 0 (2024) 1–31. <https://doi.org/10.1177/08927057241255883>.
- [21] A. Dey, I.N.R. Eagle, N. Yodo, A review on filament materials for fused filament fabrication, *Journal of Manufacturing and Materials Processing* 5 (2021). <https://doi.org/10.3390/jmmp5030069>.
- [22] I. Velghe, B. Buffel, V. Vandeginste, W. Thielemans, F. Desplentere, Effect of melt processing conditions on the degradation of PLA during single-screw extrusion, in: 2024: p. 140003. <https://doi.org/10.1063/5.0205344>.
- [23] Q. Duan, L. Meng, H. Liu, L. Yu, K. Lu, S. Khalid, L. Chen, One-Step Extrusion to Minimize Thermal Decomposition for Processing PLA-Based Composites, *J Polym Environ* 27 (2019) 158–164. <https://doi.org/10.1007/s10924-018-1323-3>.
- [24] S.W. Lo, Y.H. Lu, Wire drawing dies with prescribed variations of strain rate, *J Mater Process Technol* 123 (2002) 212–218. [https://doi.org/10.1016/S0924-0136\(02\)00033-X](https://doi.org/10.1016/S0924-0136(02)00033-X).
- [25] C. Amnael Orozco-Díaz, R. Moorehead, G.C. Reilly, F. Gilchrist, C. Miller, Characterization of a composite polylactic acid-hydroxyapatite 3D-printing filament for bone-regeneration, *Biomed Phys Eng Express* 7 (2020) 25007. <https://doi.org/10.1088/2057-1976/ab73f8>.
- [26] M.P. Bernardo, B.C.R. da Silva, L.H.C. Mattoso, Development of three-dimensional printing filaments based on poly(lactic acid)/hydroxyapatite composites with potential for tissue engineering, *J Compos Mater* 55 (2021) 2289–2300. <https://doi.org/10.1177/0021998320988568>.
- [27] İ. Kaya, M.C. Şahin, İ.D. Cingöz, N. Aydın, M. Atar, C. Kizmazoğlu, S. Kavuncu, H.E. Aydın, Three dimensional printing and biomaterials in the repairment of bone defects; hydroxyapatite pla filaments, *Turk J Med Sci* 49 (2019) 922–927. <https://doi.org/10.3906/sag-1901-184>.
- [28] J. Aniulis, G. Dudzik, K.M. Abramski, Automated non-destructive 3D printing filament material properties monitoring based on electric permittivity, longitudinal encoding and diameter multi-axes real-time measurements, *Addit Manuf* 84 (2024). <https://doi.org/10.1016/j.addma.2024.104103>.
- [29] J. Walker, M. Melaj, R. Giménez, E. Pérez, C. Bernal, Solid-State Drawing of Commercial Poly(Lactic Acid) (PLA) Based Filaments, *Front Mater* 6 (2019). <https://doi.org/10.3389/fmats.2019.00280>.
- [30] R.S. Porter, New Developments in Solid-State Extrusion, *Journal of Macromolecular Science, Part B* 19 (1981) 377–386. <https://doi.org/10.1080/00222348108015309>.
- [31] A. Das, D. Pamu, A comprehensive review on electrical properties of hydroxyapatite based ceramic composites, *Materials Science and Engineering C* 101 (2019) 539–563. <https://doi.org/10.1016/j.msec.2019.03.077>.

- [32] S.I. Platov, V.A. Nekit, N.N. Ogarkov, Determination of frictional forces during wire rod drawing process by reverse method, in: *Solid State Phenomena*, Trans Tech Publications Ltd, 2017: pp. 1152–1156. <https://doi.org/10.4028/www.scientific.net/SSP.265.1152>.
- [33] D. Sawai, K. Takahashi, T. Imamura, K. Nakamura, T. Kanamoto, S.-H. Hyon, Preparation of Oriented-Form Poly(L-lactic acid) by Solid-State Extrusion, *J Polym Sci Part B: Polym Phys* 40 (2002) 95–104. <https://doi.org/10.1002/polb.0000>.
- [34] T. Shimada, A.E. Zachariades, M.P.C. Watts, R.S. Porter, Push-Pull Extrusion: A New Approach for the Solid-State Deformation Illustrated with High Density Polyethylene, n.d.
- [35] M. Droscher, Solid-state extrusion of semicrystalline copolymers, (1982) 119–138. <https://doi.org/10.1007/BFB0038533>.
- [36] P.R. a. s. E3D, Prusa Nozzle Data Sheet, <https://E3d-Online.Com/Pages/Prusa-Nextruder-Nozzle-Datasheet> (2024).
- [37] M. Moretti, A. Rossi, N. Senin, In-process simulation of the extrusion to support optimisation and real-time monitoring in fused filament fabrication, *Addit Manuf* 38 (2021). <https://doi.org/10.1016/j.addma.2020.101817>.
- [38] W. Li, W. Liu, F. Qian, P. Mao, J. Wang, Microstructural evolution of AA7050 alloy wires during tandem hot rolling (THR) and cold-drawing process, *Materials Science and Engineering: A* 849 (2022). <https://doi.org/10.1016/j.msea.2022.143512>.
- [39] G. Vega, A. Haddi, A. Imad, Investigation of process parameters effect on the copper-wire drawing, *Mater Des* 30 (2009) 3308–3312. <https://doi.org/10.1016/j.matdes.2008.12.006>.
- [40] W. Wasserbäch, W. Skrotzki, P. Chekhonin, Strengthening of ods silver wires, *Materialia (Oxf)* 12 (2020). <https://doi.org/10.1016/j.mtla.2020.100818>.
- [41] A. Rudolf, J. Geršak, M.S. Smole, The effect of heat treatment conditions using the drawing process on the properties of PET filament sewing thread, *Textile Research Journal* 82 (2012) 161–171. <https://doi.org/10.1177/0040517511413318>.
- [42] Jakub Aniulis, Uklad do Pomiaru Wzgleđnej Przenikalności Dielektrycznej Materialu Stosowanego w Urządzeniu Wytwarzania Przyrostowego, Patent, Poland, P.442152, 2022.
- [43] S.D. Sanladerer Thomas, Inline filament diameter estimator, lowcost (InFiDEL), <https://Github.Com/Drspangle/Infidel-Sensor> (2021).
- [44] G.C. Dubbeldam, Laser Shadow Method For Measuring The Diameter Of A Transparent Filament, <https://Doi.Org/10.1117/12.952402> 0599 (1986) 370–373. <https://doi.org/10.1117/12.952402>.
- [45] H.H. Ovrebo, S.A. Koldre, O.S. Nesheim, S.W. Eikevåg, M. Steinert, C.W. Elverum, CREATING AN OPEN-SOURCE, LOW-COST COMPOSITE FEEDER DESIGN TO IMPROVE FILAMENT QUALITY OF HIGH-PERFORMANCE MATERIALS TO BE USED IN FUSED FILAMENT FABRICATION (FFF), in: *Proceedings of the Design Society*, Cambridge University Press, 2023: pp. 1097–1106. <https://doi.org/10.1017/pds.2023.110>.
- [46] J.A. Cicero, J.R. Dorgan, J. Garrett, J. Runt, J.S. Lin, Effects of molecular architecture on two-step, melt-spun poly(lactic acid) fibers, *J Appl Polym Sci* 86 (2002) 2839–2846. <https://doi.org/10.1002/app.11268>.

- [47] G., & P.A. Meinel, Plastic deformation of polyethylene: IV. Rolling of polyethylene., *Kolloid-Zeitschrift Und Zeitschrift Für Polymere* 242 (1970) 1151–1160.
- [48] S.M. Tang, P. Cheang, M.S. AbuBakar, K.A. Khor, K. Liao, Tension-tension fatigue behavior of hydroxyapatite reinforced polyetheretherketone composites, *Int J Fatigue* 26 (2004) 49–57. [https://doi.org/10.1016/S0142-1123\(03\)00080-X](https://doi.org/10.1016/S0142-1123(03)00080-X).
- [49] L. Qi, L. Ju, J. Zhou, S. Li, T. Zhang, W. Tian, Tensile and fatigue behavior of carbon fiber reinforced magnesium composite fabricated by liquid-solid extrusion following vacuum pressure infiltration, *J Alloys Compd* 721 (2017) 55–63. <https://doi.org/10.1016/j.jallcom.2017.05.312>.
- [50] N., K.T., S.S., & K.O. Sato, Microfailure behaviour of randomly dispersed short fibre reinforced thermoplastic composites obtained by direct SEM observation., *J Mater Sci* 26 (1991) 3891–3898.
- [51] S. Wang, B. Liu, Y. Qin, H. Guo, Effects of processing conditions and plasticizing-reinforcing modification on the crystallization and physical properties of pla films, *Membranes (Basel)* 11 (2021). <https://doi.org/10.3390/membranes11080640>.
- [52] F. Perrin, M.N. Bureau, J. Denault, J.I. Dickson, Mode I interlaminar crack propagation in continuous glass fiber/polypropylene composites: temperature and molding condition dependence, *Compos Sci Technol* 63 (2003) 597–607. [https://doi.org/10.1016/S0266-3538\(02\)00255-5](https://doi.org/10.1016/S0266-3538(02)00255-5).
- [53] T. Péter, K. Litauszki, Á. Kmetty, Improving the heat deflection temperature of poly(lactic acid) foams by annealing, *Polym Degrad Stab* 190 (2021). <https://doi.org/10.1016/j.polymdegradstab.2021.109646>.
- [54] A.J. Antończak, M. Wieczorek, P. Dzienny, B. Kryszak, A. Krokos, P. Gruber, M. Olejarczyk, M. Gazińska, First, do not degrade – Dual Beam Laser Sintering of polymers, *Addit Manuf* 53 (2022) 1–14. <https://doi.org/10.1016/j.addma.2022.102715>.
- [55] T. Guo, S. Zhou, X. Zheng, J. Jiang, Modeling and investigation of interfacial interaction between PLA and one type of deficient hydroxyapatite., *J Phys Chem A* 113 (2009) 7112–7123. <https://doi.org/10.1021/jp9017234>.
- [56] S. Zhou, X. Zheng, X. Yu, J. Wang, J. Weng, X. Li, B. Feng, M. Yin, Hydrogen bonding interaction of poly(D,L-lactide)/hydroxyapatite nanocomposites, *Chemistry of Materials* 19 (2007) 247–253. <https://doi.org/10.1021/cm0619398>.
- [57] J.M. Ferri, J. Jordá, N. Montanes, O. Fenollar, R. Balart, Manufacturing and characterization of poly(lactic acid) composites with hydroxyapatite, *Journal of Thermoplastic Composite Materials* 31 (2018) 865–881. <https://doi.org/10.1177/0892705717729014>.
- [58] C. Pereira, A. Ramalho, J. Ambrosio, An enhanced cylindrical contact force model, *Multibody Syst Dyn* 35 (2015) 277–298. <https://doi.org/10.1007/s11044-015-9463-x>.
- [59] H. Singh, Planar Equilibria of an Elastic Rod Wrapped Around a Circular Capstan, *J Elast* 151 (2022) 321–346. <https://doi.org/10.1007/s10659-022-09939-8>.
- [60] The transverse compression of anisotropic fibre monofilaments, *Proc R Soc Lond A Math Phys Sci* 285 (1965) 275–286. <https://doi.org/10.1098/rspa.1965.0103>.

- [61] L.K. Hillbrick, J. Kaiser, M.G. Huson, G.R.S. Naylor, E.S. Wise, A.D. Miller, S. Lucas, Determination of the transverse modulus of cylindrical samples by compression between two parallel flat plates, *SN Appl Sci* 1 (2019). <https://doi.org/10.1007/s42452-019-0726-7>.
- [62] C.M. Pereira, A.L. Ramalho, J.A. Ambrósio, A critical overview of internal and external cylinder contact force models, *Nonlinear Dyn* 63 (2011) 681–697. <https://doi.org/10.1007/s11071-010-9830-3>.
- [63] T. Pícha, S. Papežová, Dielectric properties of materials for 3D printing at high frequencies, *Research in Agricultural Engineering* 69 (2023) 28–35. <https://doi.org/10.17221/10/2022-RAE>.
- [64] T. Pícha, S. Papežová, S. Pícha, Evaluation of Relative Permittivity and Loss Factor of 3D Printing Materials for Use in RF Electronic Applications, *Processes* 10 (2022). <https://doi.org/10.3390/pr10091881>.
- [65] D. Kalaš, K. Šíma, P. Kadlec, R. Polanský, R. Soukup, J. Řeboun, A. Hamáček, Fff 3d printing in electronic applications: Dielectric and thermal properties of selected polymers, *Polymers (Basel)* 13 (2021). <https://doi.org/10.3390/polym13213702>.
- [66] Z. Zhu, Y. Bian, X. Zhang, R. Zeng, B. Yang, Study of Crystallinity and Conformation of Poly(lactic acid) by Terahertz Spectroscopy, *Anal Chem* 94 (2022) 11104–11111. <https://doi.org/10.1021/acs.analchem.2c02652>.
- [67] A. Kumar, S. Kargozar, F. Baino, S.S. Han, Additive Manufacturing Methods for Producing Hydroxyapatite and Hydroxyapatite-Based Composite Scaffolds: A Review, *Front Mater* 6 (2019). <https://doi.org/10.3389/fmats.2019.00313>.
- [68] Jakub Vávra, Institute of Anatomy First Faculty of Medicine Charles University, Thigh Bone Scan - Femur, <https://www.printables.com/model/681332-Thigh-Bone-Scan-Femur> (2023).